

Development, intercomparison and evaluation of an improved mechanism for the oxidation of dimethyl sulfide in the UKCA model

Ben A. Cala^{1,*}, Scott Archer-Nicholls^{1,#}, James Weber^{1,§}, N. Luke Abraham^{1,2}, Paul T. Griffiths^{1,2}, Lorrie Jacob¹, Y. Matthew Shin¹, Laura E. Revell³, Matthew Woodhouse⁴, Alexander T. Archibald^{1,2}

¹Yusuf Hamied Department of Chemistry, University of Cambridge, Cambridge, CB2 1EW, UK

²National Centre for Atmospheric Science, Cambridge, CB2 1EW, UK.

³School of Physical and Chemical Sciences, University of Canterbury, Christchurch, New Zealand.

⁴CSIRO Oceans and Atmosphere, Aspendale, 3195, Australia.

*Now at Department of Ocean Systems (OCS), NIOZ Royal Netherlands Institute for Sea Research, Texel, the Netherlands

#Now at IT Services, University of Manchester, Manchester, M13 9PL, UK.

§Now at School of Biosciences, University of Sheffield, S10 2TN, UK.

Correspondence to: Alexander T. Archibald ata27@cam.ac.uk and Ben. A. Cala ben.cala@nioz.nl

Abstract. Dimethyl sulfide (DMS) is an important trace gas emitted from the ocean. The oxidation of DMS has long been recognised as being important for global climate through the role DMS plays in setting the sulfate aerosol background in the troposphere. However, the mechanisms in which DMS is oxidised are very complex and have proved elusive to accurately determine in spite of decades of research. As a result the representation of DMS oxidation in global chemistry-climate models is often greatly simplified.

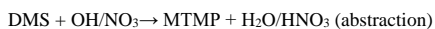
Recent field observations, laboratory and ab initio studies have prompted renewed efforts in understanding the DMS oxidation mechanism, with implications for constraining the uncertainty in the oxidation mechanism of DMS as incorporated in global chemistry-climate models. Here we build on recent evidence and develop a new DMS mechanism for inclusion in the UK [Chemistry Aerosol \(UKCA\)](#) chemistry-climate model. We compare our new mechanism (CS2-HPMTF) to a number of existing mechanisms used in UKCA (including the highly simplified 3 reactions, 2 species, ~~ST~~-mechanism used in CMIP6 studies [with the model](#)) and to a range of recently developed mechanisms reported in the literature through a series of global and box model experiments. Global model runs with the new mechanism enable us to simulate the global distribution of hydroperoxyl methyl thioformate (HPMTF), which we calculate to have a burden of 2.6-26 Gg S (in good agreement with the literature range of 0.7-18 Gg S). We show that the sinks of HPMTF dominate uncertainty in the budget, not the rate of the isomerisation reaction forming it, and that based on the observed DMS/HPMTF ratio [from the global surveys during the NAS Atmospheric Tomography mission \(ATom\)](#), rapid cloud uptake of HPMTF worsens the model-observation comparison. Our box model experiments highlight that there is significant variance in simulated secondary oxidation products from DMS across mechanisms used in the literature, with significant divergence in the [rates of formation of these](#) products to

Development and intercomparison of DMS oxidation mechanisms

34 temperature exhibited; especially for methane sulfonic acid (MSA). Our global model studies show that our updated DMS
35 scheme performs better than the current scheme used in UKCA when compared against a suite of surface and aircraft
36 observations. However, sensitivity studies underscore the need for further laboratory and observational constraints.

37 **1 Introduction**

38 It is estimated that 16-28 Tg S year⁻¹ are emitted in the form of dimethyl sulfide (DMS, CH₃SCH₃) from the ocean, making
39 DMS the most abundant biological source of sulfur in the Earth system (Andreae, 1990, Tesdal et al., 2015, Bock et al., 2021).
40 Elucidating the atmospheric fate of DMS has been a long standing goal of the atmospheric chemistry research community
41 owing to a proposed biogeochemical feedback cycle (CLAW; Charlson et al. 1987), whereby DMS oxidation is key to a
42 homeostatic feedback loop. The initial steps in DMS oxidation are well understood (Barnes et al., 2006). Focusing on oxidation
43 via OH (NO₃), the most important oxidant during the daytime (nighttime), DMS is oxidised in the gas-phase through two main
44 pathways: the abstraction pathway forms the methylthiomethylperoxy radical (MTMP, CH₃SCH₂OO) in the first step, while
45 the addition pathway leads to dimethyl sulfoxide (DMSO, CH₃SOCH₃; and to a lesser extent DMSO₂) as an important
46 intermediate.

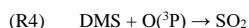
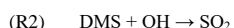
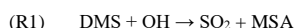


49 Ultimately, the oxidation of DMS leads to products such as H₂SO₄ and sulfate (SO₄²⁻), as these represent the highest oxidation
50 states of sulfur (S(VI)). Along the way from DMS, a number of secondary oxidation products such as sulfur dioxide (SO₂),
51 methane sulfonic acid (MSA, CH₃SO₃H) and carbonyl sulfide (OCS) can be formed, however the yields of these species
52 depend on the mechanisms involved, which themselves are a function of the chemical (e.g., levels of oxidants) and
53 environmental conditions (e.g., temperature and humidity). The yields of these products are relatively uncertain, with estimates
54 of the DMS-to-SO₂ yield spanning 14-96 % (von Glasow and Crutzen, 2014). The oxidation products can participate in
55 aerosol growth and in new particle formation, affecting the number of cloud condensation nuclei (CCN). As such DMS
56 oxidation can impact cloud formation and lifetime and hence climate; although the absolute effect is still highly uncertain due
57 to the uncertainty in [the kinetics and mechanisms of DMS oxidation](#). Indeed, natural aerosols such as DMS contribute to large
58 uncertainties in the radiative forcing of the pre-industrial atmosphere (Carslaw et al., 2013; Fung et al., 2022).

59
60 Substantial discrepancies between different DMS oxidation mechanisms under different conditions have been found (de Bryn
61 et al., 2002; von Glasow and Crutzen, 2004). The intercomparison study by Karl et al. (2007) looked at ~~six~~-seven different
62 chemistry schemes in a box model ([using the same inputs](#)) and observed that SO₂ mixing ratios varied from 2 to 44 ppt.
63 Differences between models are even greater when looking at MSA yield (Karl et al., 2007, Hoffmann et al., 2021). The large
64 uncertainties of product ratios indicate the need for more observational constraints for DMS chemistry in models.

Development and intercomparison of DMS oxidation mechanisms

In the UK Chemistry and Aerosol model (UKCA) two different chemistry schemes are implemented: StratTrop (Archibald et al., 2020), which is a simplified chemistry mechanism included in the UK Earth System Model (Sellar et al., 2019) and CRI-Strat2 (Archer Nicholls et al., 2021; Weber et al., 2021). The DMS oxidation mechanism in StratTrop is, like those used in many Earth System Models (ESMs), a very simple scheme (see S1.4.1 for more details). We believe modellers have opted to keep the DMS chemistry incredibly simple for two main reasons 1) numerical efficiency 2) uncertainty in what to do owing to lack of detailed DMS oxidation mechanisms that have been calibrated against laboratory data. The StratTrop DMS mechanism only includes four reactions and no intermediates for the DMS oxidation scheme.



Omitting intermediates might lead to a misrepresentation of the spatial distribution of oxidation products and an overestimation in their formation since the intermediates might be subject to wet and dry deposition or cloud uptake. Because a unity yield of SO_2 is assumed, a change in the distribution of oxidation products due to a changing climate cannot be evaluated.

CRI-Strat2 (hereafter CS2) (Archer-Nicholls et al., 2021, Weber et al., 2021) is a mechanism that aims to be of intermediate complexity. CS2 includes 19 reactions and 7 intermediates (DMSO, MSIA, MTMP, CH_3S , CH_3SO , CH_3SO_2 , CH_3SO_3) as part of its DMS scheme and is primarily based on the work of von Glasow and Crutzen (2004). Whilst the CS2 DMS mechanism is much more complex than the StratTrop scheme, it represents an understanding of DMS chemistry that is far from up-to-date.

In this work, the gas-phase DMS oxidation by OH and NO_3 in CS2 is updated according to the current scientific understanding. The greatest update is the inclusion of the recently discovered intermediate hydroperoxymethyl thioformate (HPMTF, HOCH_2SCHO), which is formed through the autoxidation of the methylthiomethyl peroxy radical (MTMP, $\text{CH}_3\text{SCH}_2\text{OO}$) in the abstraction pathway (Wu et al., 2015, Berndt et al., 2019, Veres et al. 2020). Currently, it is estimated that ~30–45% of DMS yields HPMTF (Veres et al., 2020; Novak et al. (2021); Fung et al. (2022)). There are large uncertainties about the value of $k_{\text{isom},1}$, the rate constant of the first H-shift, which is the rate determining step for HPMTF formation (Figure 1). (Note, given that the first isomerization step is rate limiting, the overall rate constant for isomerization is denoted k_{isom}). This determines if autoxidation can compete with or surpass the bimolecular reactions of MTMP with HO_2 and NO. The chamber study by Ye et al. (2021) estimates a probability distribution based on their measurements with one geometric standard deviation spanning an order of magnitude. The isomerization rate constant is predicted using *ab initio* methods to be strongly temperature dependent, indicating that this pathway could be more relevant under a warming climate (Wu et al., 2015; Veres et al., 2020). Following the closure of the Discussion version of this manuscript the first temperature-dependent direct kinetic study of the isomerization

Formatted: Font: Italic

Formatted: Font: Italic, Subscript

Development and intercomparison of DMS oxidation mechanisms

98 [of rate constant for MTMP to HPMTF was published \(Assaf et al., 2023\). In that study the authors calculate the Arrhenius](#)
99 [temperature barrier as \$7278 \pm 99\$ K, confirming the high temperature dependence of the reaction experimentally.](#)

100
101 As of now, the fate of HPMTF in the atmosphere is largely unknown. Wu et al. (2015) postulate further oxidation with OH,
102 ultimately yielding SO₂ as the dominant product and OCS as a side product. Veres et al. (2020) observe an abrupt decrease of
103 HPMTF mixing ratio in clouds and therefore suggest that heterogeneous loss to aerosol and cloud uptake plays a big role.
104 Vermeuel et al. (2020) support this hypothesis: they find a diurnal profile of HPMTF in the vicinity of California's coast and
105 suggest this is due to the consistent diurnal profile of cloud present. This hypothesis is further supported by the study by Novak
106 et al. (2021), which looks at two case studies and concludes that cloud uptake determines the lifetime of HPMTF. Novak et
107 al. (2021) found that cloud-uptake of HPMTF reduces SO₂ production from DMS by over a third, while providing a more
108 direct pathway to sulfate formation. On the contrary, the chamber study and calculation of Henry's law constant by Wollesen
109 de Jonge et al. (2021) predict that HPMTF does not directly contribute to new particle formation or aerosol growth. Instead,
110 their study proposes aqueous oxidation by OH, ultimately still yielding gas-phase SO₂. Khan et al. (2021) stress the importance
111 of photolysis as a potential loss pathway, which might explain the observed diurnal concentrations throughout the day. Overall,
112 loss processes of HPMTF are poorly understood.

113
114 In this work, we perform a series of updates to the CS₂ DMS oxidation scheme which are evaluated against the current CS₂
115 and the very simplified DMS chemistry in StratTrop. The aim of this work is to improve the representation of DMS chemistry
116 in UKCA and determine the influence of some of the major mechanistic uncertainties on model simulated SO₂ levels compared
117 against ATom observations (Wofsy et al., 2018; Veres et al., 2020). Our study includes a comprehensive set of box model
118 studies, including an intercomparison of our new DMS scheme against other recently reported schemes in the literature, and
119 global 3D simulations with the UKCA model. [To complement the work of Fung et al. \(2022\),](#) ~~S~~sensitivity studies with ~~slower~~
120 ~~loss, a faster~~[variable rates of](#) production, and cloud and aerosol uptake of HPMTF are performed to investigate the effects of
121 the uncertainty in HPMTF formation and depletion on the distribution and burden of SO₂ and sulfate (given their importance
122 in climate) [using a structurally different model to that they used.](#)

2 Methods

2.1 Model description

2.1.1 Set up

Box model

For the box model experiments, BOXMOX (Knote et al., 2015), the box modelling extension to the Kinetic PreProcessor (KPP) (Sandu and Sander, 2006) was used. The initial and background concentrations of the species were set to be representative of the remote marine boundary layer (MBL) (and are detailed in **Table S1**). NO_x concentration was kept at approximately 10 ppt, unless otherwise specified.

The box model set up simulates an MBL air parcel exchanging with the free troposphere. The diurnal profile of the planetary boundary layer height was modelled after the diurnal profile of the MBL in Ho et al. (2015) (**Table S2**). Mixing of the air within the box with the free troposphere is described by the increases of box height: it is assumed that changes in the box volume are due to the influx of background air. Emissions of DMS are added at $3.48 \times 10^9 \text{ molec. cm}^{-2} \text{ s}^{-1}$ (consistent with von Glasow and Crutzen, 2004). Emissions mix instantaneously within the box. Temperature varies throughout a 24-hour period between 289–297 K, with a mean of 293 K (**Table S2**). Photolysis reactions are scaled depending on the time of day, and make use of the pre-calculated “J” rates obtained from the MCMv3.3.1. The simulations were run for 192 hours (8 days) with 10-minute time steps. CRI v2.2 R5 (CS2) (Jenkin et al., 2019; Weber et al., 2021) was employed as the base chemical mechanism. Unless otherwise specified, only reactions of the DMS scheme were changed. Neither dry nor wet deposition was included in the box model experiments. The analysis of the BOXMOX simulations discussed in Section 3.1.1 and 3.2.1 focuses on the continuous (hourly) output. In Section 3.1.2 and 3.2.2, simulations with a prescribed temperature (260 - 310 K, step size: 5 K) were conducted. The data from day 7 and 8 of the runs was averaged to enable the effects of changes in the temperature on species concentration simulated in the box model to be calculated (following Archibald et al., 2010)

3D simulations

For the 3D simulations we use UKCA, the chemistry and aerosol component of UKESM1, [with a horizontal resolution of \$1.25^\circ \times 1.875^\circ\$ with 85 vertical levels up to 85 km \(Walters et al., 2019\)](#), ~~and the UKCA uses the~~ GLOMAP-mode aerosol scheme, which simulates sulfate, sea salt, black carbon (BC), organic matter, and dust but does not [currently simulate currently](#) nitrate aerosol (Mulcahy et al., 2020). Simulations were run for 18 months, using the first 6 months as spin up. In order to look at high time resolution output simulations were re-run for limited time periods using the re-start files of the longer runs but outputting data at hourly frequency.

Temperature and horizontal wind fields were nudged (Telford et al., 2013) in all model runs to the Era-Interim atmospheric reanalysis from ECMWF (Dee et al., 2011). [See the SI for further details. This constrains the different simulations to consistent meteorology, thus preventing differences in meteorology complicating the attribution of differences resulting from the](#)

Development and intercomparison of DMS oxidation mechanisms

157 ~~chemical mechanism changes, and replicating the atmospheric conditions experienced when the observations were recorded~~
158 ~~as closely as possible. Nudging only occurred above ~1200 m in altitude, and thus the majority of the planetary boundary layer~~
159 ~~was not nudged. The model runs were atmosphere-only runs with prescribed sea surface temperatures (SSTs). CO₂ is not~~
160 ~~emitted but set to a constant field, while methane, CFCs, and N₂O are prescribed with constant lower boundary conditions, all~~
161 ~~at 2014 levels (Archibald et al., 2020).~~

162
163 The emissions used in this study for UKCA are the same as those from Archer-Nicholls et al (2021) and are those developed
164 for the Coupled-Model Intercomparison Project 6 (CMIP6) (Collins et al., 2017). ~~See the SI for further details. Anthropogenic~~
165 ~~and biomass burning emissions data (including DMS) for CMIP6 are from the Community Emissions Data System (CEDS),~~
166 ~~as described by Hoesly et al. (2018). All runs used time slice 2014 emissions for anthropogenic and biomass burning emissions.~~
167 ~~Oceanic emissions of CO₂, C₂H₄, C₂H₆, C₃H₆ and C₄H₈ were from the POET 1990 data set (Olivier et al., 2003), and all~~
168 ~~terrestrial biogenic emissions except isoprene and monoterpenes were based on 2001–2010 climatologies from Model of~~
169 ~~Emissions of Gases and Aerosols from Nature under the Monitoring Atmospheric Composition and Climate project (MEGAN-~~
170 ~~MACC) (MEGAN) version 2.1 (Guenther et al., 2012). Emissions of isoprene and monoterpenes were simulated by the~~
171 ~~interactive biogenic volatile organic compound (iBVOC) emissions system (Pacífico et al., 2011), the standard approach for~~
172 ~~UKESM1's contributions to CMIP6 (Sellar et al., 2019). Emissions of isoprene and monoterpenes are calculated interactively~~
173 ~~based on temperature, CO₂, photosynthetic activity and plant functional types for each grid cell. Oceanic emissions of DMS~~
174 ~~are calculated from seawater DMS concentrations (Sellar et al., 2019). In the atmosphere-only setup employed here seawater~~
175 ~~DMS concentrations for 2014 from a UKESM1 fully-coupled SSP3-70 ensemble member were prescribed. The DMS emission~~
176 ~~flux from the ocean used in the model was 16 Tg S yr⁻¹ and therefore on the low end of estimates of oceanic DMS emissions~~
177 ~~(e.g., Lana et al., 2011; Bock et al., 2021).~~

178
179 ~~While the StratTrop mechanism and the variants of the CS2 mechanism all use the same raw emissions data, the additional~~
180 ~~emitted species required by CS2 means the total mass of emitted organic compounds is greater in CS2, and the lumping of~~
181 ~~species for emissions is also different. The approach and consequences are discussed in Archer-Nicholls et al (2021).~~

2.1.2 Model runs

182
183
184
185 **Table 1:** Configuration of model runs in this study. The last two columns indicate whether this scheme was used for the
186 BOXMOX experiments or the UKCA runs or both. Additional BOXMOX simulations were performed and the results of which
187 are included in the Supplementary Information (SI) for completeness.

Used for:

Development and intercomparison of DMS oxidation mechanisms

Alias	Description	BOXMOX	UKCA
CS2	Base simulation, standard CRIStrat2 (or CRIV2.2R5) scheme	✓	✓
ST	StratTrop chemistry scheme ($ST - CS2 = \Delta ST$; change between ST and CS2)	✓	✓
ST~CS2	StratTrop DMS scheme but CS2 oxidants ($ST - CS2 - CS2 = \Delta CC$; change between CS2 and the ST DMS scheme only)	✓	-
CS2-HPMTF	CS2 + updates in Table 2 and Table 3 ($CS2 - HPMTF - CS2 = \Delta UPD$; effects of all updates ^{s4} made to the scheme)	✓	✓
CS2-UPD-DMS	CS2 + updates in Table 2 = CS2-HPMTF - updates in Table 3 ($CS2 - HPMTF - CS2 - UPD - DMS = \Delta HPMTF$; effects of the isom. <u>p</u> pathway only)	✓	-
CS2-HPMTF-CLD	CS2-HPMTF + cloud and aerosol uptake ($\gamma = 0.01$) ($CS2 - HPMTF - CLD - CS2 - HPMTF = \Delta CLD$; gives the effects of cloud and aerosol uptake of HPMTF)	-	✓
CS2-HPMTF-FL	CS2-HPMTF + faster total loss of HPMTF to OH ($5.5 \times 10^{-11} \text{ s}^{-1}$) ($CS2 - HPMTF - FL - CS2 - HPMTF = \Delta FL$; gives the effects of faster gas phase loss of HPMTF)	SI	✓
CS2-HPMTF-FP	CS2-HPMTF + isomerisation A-factor scaled by a factor of 5, see Wollesen de Jonge et al. (2021) ($CS2 - HPMTF - FP - CS2 - HPMTF = \Delta FP$; gives the effects of faster HPMTF production)	SI	✓

188

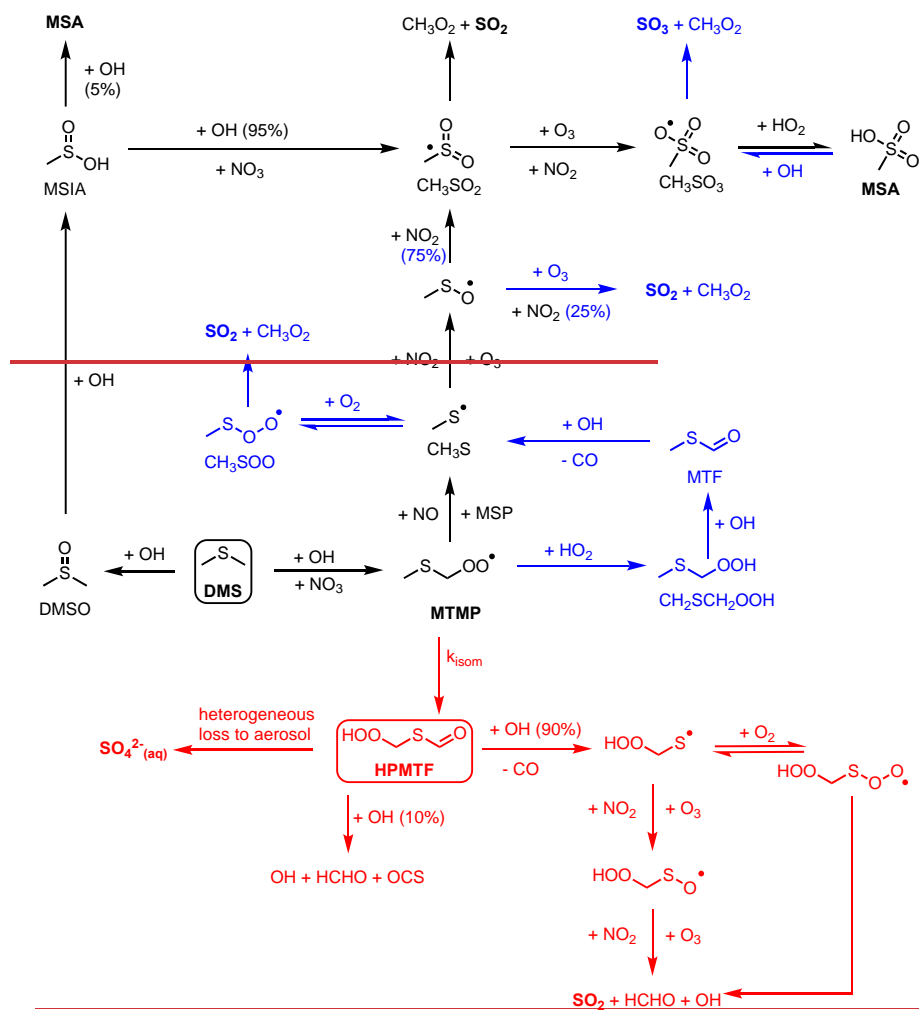
189 Simulations are performed with the standard or updated DMS scheme to quantify the impacts of the mechanistic changes.
 190 Details are given in **Table 1**. We chose as our base run a simulation with the CRIStrat2 chemistry scheme hereafter referred
 191 to as CS2 (Weber et al., 2021). We perform two simulations with StratTrop (hereafter ST): ST is the default mechanism as
 192 used in UKESM1, while ST~CS2 uses the ST DMS chemistry (R1-R4) but all other reactions (HO_x , NO_x , VOC etc) are
 193 identical to CS2. This allows us to attribute the changes arising solely to differences in the oxidising capacity/environment
 194 (driven by the chemistry not strongly coupled to DMS) and isolate the role due to differences in the DMS reactions themselves.
 195

196 In updating the representation of DMS chemistry for UKCA a number of changes were considered. Broadly these fall into two
 197 categories: 1) Incorporation of the chemistry of HPMTF (shown in red in **Figure 1**) 2) updates to other aspects of DMS
 198 oxidation chemistry (shown in blue in **Figure 1**). CS2-HPMTF is used to identify the fully updated DMS mechanism (**Table**
 199 **2**, **Table 3**). All other runs act as sensitivity runs. CS2-UPD-DMS allows the evaluation of only updating the standard DMS
 200 chemistry (**Table 2**), without the addition of the isomerization branch and HPMTF formation (**Table 3**). CS2-HPMTF-CLD
 201 adds cloud and aerosol uptake of HPMTF with subsequent sulfate formation, similar to Novak et al. (2021). With CS2-
 202 HPMTF-FP and CS2-HPMTF-FL the effects of faster production and faster loss of HPMTF can be assessed.
 203

Development and intercomparison of DMS oxidation mechanisms

204

Development and intercomparison of DMS oxidation mechanisms



Development and intercomparison of DMS oxidation mechanisms

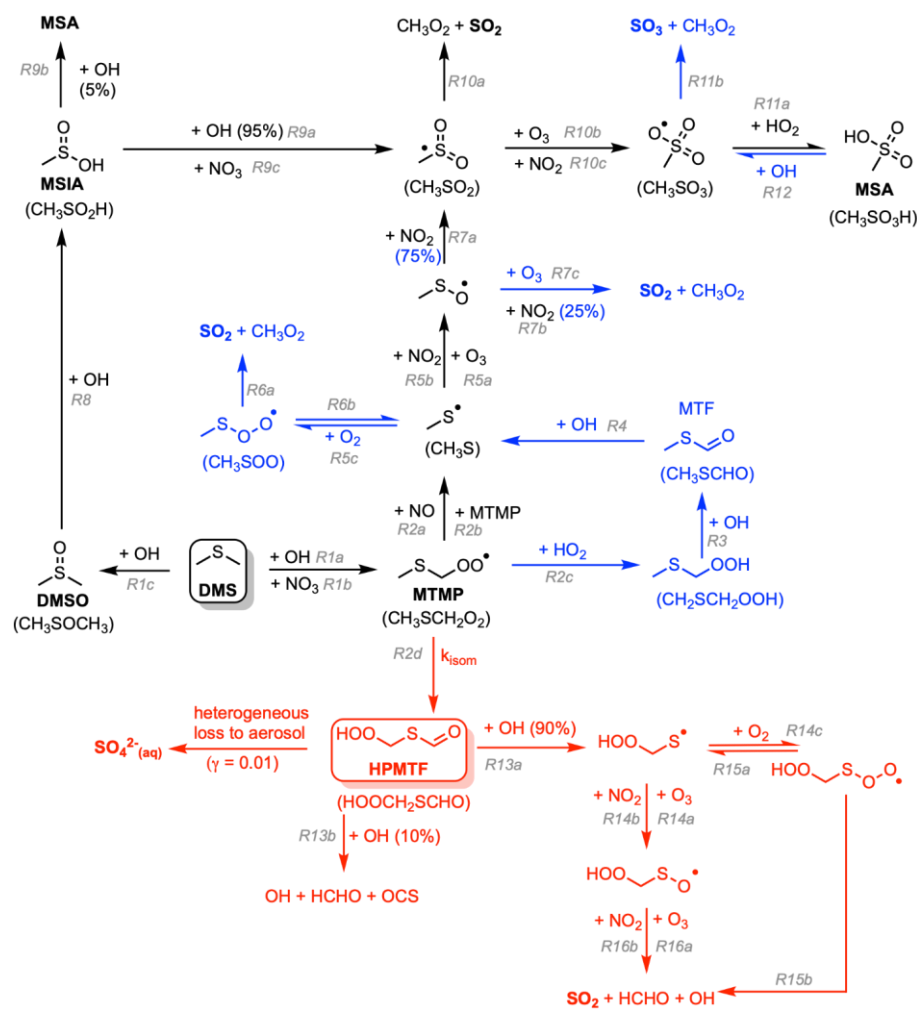


Figure 1. Schematic summary of the changes and additions to the gas-phase DMS oxidation mechanism in CS_2 . The current chemistry in CS_2 (Weber et al., 2021) is in black, changes associated with CS_2 -UPD-DMS are shown in blue and changes associated with the addition of the isomerization pathway for CS_2 -HPMTF in red.

2.2 New mechanism development

The current CS₂ DMS oxidation mechanism is based on von Glasow and Crutzen (2004). This mechanism is based on an outdated understanding of DMS oxidation, which excludes key pathways and intermediates that are now known to be well established (Barnes et al., 2006) as well as more recent pathways and products that have been shown to be important (Veres et al., 2020). Our aim with the development of the new mechanism is to build upon the existing mechanism in CS₂ and to update and extend it. To this end we performed a literature review and constructed a number of mechanistic variants that were examined in a series of box model experiments. As with all mechanism development exercises a series of target compounds were chosen to reduce the mechanism to achieve a scheme that is parsimonious; for use in a 3D chemistry-climate model. In our study we chose DMS, SO₂, sulfate and HPMTF as the key target molecules for mechanism optimization. **Figure 1** shows the two-step improvement of this mechanism. First, the improvement of the standard chemistry by updating rate constants for existing reactions in the scheme or the addition of reactions that were missing (denoted with blue colouring in **Figure 1**), and second, the addition of the HPMTF pathway (in red in **Figure 1**). The focus in this study is on gas-phase DMS oxidation by OH and NO₃. Our prime focus is on the primary oxidation products (DMSO and MTMP) and their subsequent chemistry. While other studies include DMS oxidation by BrO and Cl, the contribution is either negligible or there is a large uncertainty attached due to substantial discrepancies between/within models and measurements of halogens and halogen oxides (Wang et al., 2021; Fung et al., 2022). Moreover, UKCA doesn't currently have a comprehensive tropospheric halogen mechanism and levels of BrO and Cl simulated are much lower than observations suggest.

2.2.1 Updating the standard DMS chemistry in CRIStrat 2

The H-abstraction pathway (reaction 1a,b) generates MTMP which is then further oxidised to SO₂ or CH₃SO₂ (reactions 2-7). The OH-addition pathway (reaction 1c) leads to dimethyl sulfoxide (DMSO, (CH₃)₂SO) and methanesulfinic acid (MSIA, CH₃S(O)OH) (reactions 8,9) and further oxidation through to CH₃SO₂ (reactions 10-12). Both pathways and the changes made are summarised in **Table 2**. The newly added reactions and their respective rate constants are largely based on Atkinson et al. (2004), the MCMv3.3.1 (Jenkin et al. 2015), and the primary literature therein.

The oxidation of MTMP by HO₂ (reaction 2c) was not previously included in the CS₂ mechanism, but is expected to play a significant role at the low NO_x conditions over the remote ocean. Based on other RO₂ + HO₂ reactions, CH₃SCH₂OOH is the expected product, which has been detected through mass spectroscopy (Butkovskaya and LeBras, 1994). Since no experimental measurements exist for the kinetics of this reaction, the rate constant provided in the MCM was used. It is based on a generic expression, defined on the basis of available room temperature and temperature dependent data for alkyl and β-hydroxy RO₂ and it is dependent on the number of carbon atoms. Further oxidation of CH₃SCH₂OOH leads to the formation of methylthiolformate (MTF, CH₃SCHO) (reaction 3), a species that has been detected in chamber studies before under low NO_x

Development and intercomparison of DMS oxidation mechanisms

243 conditions (Arsene et al., 1999, Urbanski et al., 1998). MTF decomposes to CH_3S (reaction 4), an intermediate that is already
244 part of the CS2 DMS scheme as a reaction product of MTMP (reaction 2a,b).

245
246 CH_3S can add an O_2 to form a weakly bound adduct, CH_3SOO (reaction 5c). At 298 K at sea level, approximately one-
247 third of CH_3S is present as the CH_3SOO adduct and at colder temperatures this ratio is even greater (75% at 273 K)
248 (Turnipseed et al., 1992). CH_3SOO can decompose to CH_3 and SO_2 (reaction 6a), which proceeds through isomerization
249 to CH_3SO_2 , followed by rapid thermal decomposition (McKee, 1993, Butkovskaya and Barnes, 2002, Chen et al. 2021).
250 Previous modelling studies, such as Hoffmann et al. (2016), include the isomerization step forming CH_3SO_2 but omit the
251 decomposition. This could lead to a higher yield of MSA in those studies.

252
253 CH_3S can also be oxidised by O_3 and NO_2 - NO_2 to CH_3SO (reaction 5a,b). Measurements by Borissenko et al. (2003) show
254 that O_3 oxidation of CH_3SO results in a 100% yield of SO_2 at pressures over 500 Torr (0.6 bar). Since the pressure in the
255 marine boundary layer where most of DMS oxidation takes place is above this threshold, the products of reaction 7c_old
256 were updated accordingly (reaction 7c). Additionally, the branching ratios of CH_3SO oxidation by NO_2 to CH_3SO_2 and
257 SO_2 were revised to also match the findings by Borissenko et al. (2003).

258
259 While some CH_3SO_2 stems from the NO_3 oxidation of CH_3SO , it is mainly formed through oxidation of MSIA (reaction
260 9a,c), especially under low NO_x conditions. CH_3SO_2 can decompose to SO_2 (reaction 10a) or be oxidised further by O_3 or
261 NO_3 to CH_3SO_3 (reaction 10b,c). CH_3SO_3 itself can react to form MSA (reaction 11a). CH_3SO_3 can also decompose to
262 SO_3 , similar to the decomposition reaction of CH_3SO_2 , although it is assumed that this reaction is more endothermic
263 (Barone et al., 1995). The rate constant cited by von Glasow and Crutzen (2004) that was previously implemented in CS2,
264 could not be found in the cited primary literature (reaction 11b_old). Here, the rate constant of the decomposition reaction
265 was updated to the rate constant used in the MCMv3.3.1, which is — as for the decomposition of CH_3SO_2 — based on
266 Barone et al. (1995). We note that a more recent study, by Cao et al. (2013), calculates the rate constant for the thermal
267 decomposition of CH_3SO_3 to be 12 s^{-1} ; a factor of 80 larger than the value adopted here based on the MCMv3.3.1.

268
269 MSA is formed either through oxidation of MSIA (reaction 9b) or through the reaction of HO_2 with CH_3SO_3 (reaction
270 11a). The default configuration of UKCA (for example as run in UKESM1) does not include any sinks for MSA and it is
271 not treated as a species, which prevents the comparison of MSA concentrations with observational results. Here, wet
272 deposition of MSA is added with a Henry's law coefficient of $1 \times 10^9 \text{ M atm}^{-1}$ (Campolongo et al., 1999; Sander 2021).

273 We note that Wollesen de Jonge et al. (2021) calculated the Henry's law coefficient to be ~~approximately two-an order of~~
274 magnitudes lower and so this might be an overestimate. Dry deposition for MSA is added based on the implemented values
275 for HCOOH in CRI. Additionally, the gas-phase oxidation of MSA by OH is added. Barnes et al. (2006) suggest this
276 pathway is expected to play a minor role.

277

Development and intercomparison of DMS oxidation mechanisms

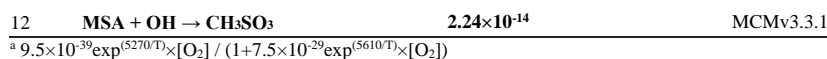
278 Wet deposition was added for MSIA with Henry's law constant of $1 \times 10^8 \text{ M atm}^{-1}$ (Barnes et al., 2006). Dry deposition is
 279 omitted for DMSO and MSIA since they are expected to be relatively short-lived.

280

281

282 **Table 2:** Summary of the H-abstraction and OH-addition branches in the DMS oxidation pathway. Reactions in **bold** are
 283 newly added in this work.

No.	Reactions	Rate ($\text{cm}^3 \text{ molecule}^{-1} \text{ s}^{-1}$)	Reference
1a	DMS + OH \rightarrow MTMP + H ₂ O	$1.12 \times 10^{-11} \exp^{(-250/T)}$	IUPAC SOx22 (upd. 2006)
1b	DMS + NO ₃ \rightarrow MTMP + HNO ₃	$1.90 \times 10^{-13} \exp^{(520/T)}$	Atkinson et al. (2004)
1c	DMS + OH \rightarrow DMSO + HO ₂	see note ^a	IUPAC SOx22 (upd. 2006)
2a	MTMP + NO \rightarrow HCHO + CH ₃ S + NO ₂	$4.90 \times 10^{-12} \exp^{(263/T)}$	von Glasow and Crutzen (2004)
2b	MTMP + MTMP \rightarrow 2 HCHO + 2 CH ₃ S	1.0×10^{-11}	von Glasow and Crutzen (2004)
2c	MTMP + HO₂ \rightarrow CH₂SCH₂OOH	$2.91 \times 10^{-13} \exp^{(1300/T)} \times 0.387$	MCMv3.3.1
3	CH₂SCH₂OOH + OH \rightarrow CH₃SCHO	7.03×10^{-11}	MCMv3.3.1
4	CH₃SCHO + OH \rightarrow CH₃S + CO	1.11×10^{-11}	MCMv3.3.1
5a	CH ₃ S + O ₃ \rightarrow CH ₃ SO	$1.15 \times 10^{-12} \exp^{(432/T)}$	Atkinson et al. (2004)
5b	CH ₃ S + NO ₂ \rightarrow CH ₃ SO + NO	$3.00 \times 10^{-12} \exp^{(210/T)}$	Atkinson et al. (2004)
5c	CH₃S + O₂ \rightarrow CH₃SOO	$1.20 \times 10^{-16} \exp^{(1580/T)} \times [\text{O}_2]$	Atkinson et al. (2004)
6a	CH₃SOO \rightarrow CH₃O₂ + SO₂	$5.60 \times 10^{-16} \exp^{(-10870/T)}$	Atkinson et al. (2004)
6b	CH₃SOO \rightarrow CH₃S + O₂	$3.50 \times 10^{-10} \exp^{(-3560/T)}$	MCMv3.3.1 (based on: McKee (1993), and Butkovskaya and Barnes (2002))
7a	CH ₃ SO + NO ₂ \rightarrow CH ₃ SO ₂ + NO	$1.2 \times 10^{-11} \times 0.75$	Borrisenko et al. (2003), Atkinson et al. (2004)
7b	CH ₃ SO + NO ₂ \rightarrow SO ₂ + CH ₃ O ₂ + NO	$1.2 \times 10^{-11} \times 0.25$	Borrisenko et al. (2003), Atkinson et al. (2004)
7c_old	CH ₃ SO + O ₃ \rightarrow CH ₃ SO ₂	6.0×10^{-13}	Von Glasow and Crutzen (2004)
7c	CH₃SO + O₃ \rightarrow CH₃O₂ + SO₂	4×10^{-13}	Borrisenko et al. (2003), IUPAC SOx61 (upd. 2006)
8	DMSO + OH \rightarrow MSIA + CH ₃ O ₂	$8.7 \times 10^{-11} \times 0.95$	von Glasow and Crutzen (2004)
9a	MSIA + OH \rightarrow CH ₃ SO ₂ + H ₂ O	$9.0 \times 10^{-11} \times 0.95$	von Glasow and Crutzen (2004)
9b	MSIA + OH \rightarrow MSA + HO ₂ + H ₂ O	$9.0 \times 10^{-11} \times 0.05$	von Glasow and Crutzen (2004)
9c	MSIA + NO ₃ \rightarrow CH ₃ SO ₂ + HNO ₃	1.0×10^{-13}	von Glasow and Crutzen (2004)
10a	CH ₃ SO ₂ \rightarrow CH ₃ O ₂ + SO ₂	$5.0 \times 10^{-13} \exp^{(-9673/T)}$	MCMv3.3.1 (based on: Barone et al. (1995))
10b	CH ₃ SO ₂ + O ₃ \rightarrow CH ₃ SO ₃	3.0×10^{-13}	von Glasow and Crutzen (2004)
10c	CH ₃ SO ₂ + NO ₂ \rightarrow CH ₃ SO ₃ + NO	2.2×10^{-12}	Atkinson et al. (2004)
11a	CH ₃ SO ₃ + HO ₂ \rightarrow MSA	5.0×10^{-11}	von Glasow and Crutzen (2004)
11b_old	CH ₃ SO ₃ \rightarrow CH ₃ O ₂ + H ₂ SO ₄	$1.36 \times 10^{14} \exp^{(-11071/T)}$	von Glasow and Crutzen (2004)
11b	CH₃SO₃ \rightarrow CH₃O₂ + SO₃	$5.0 \times 10^{13} \exp^{(-9946/T)}$	MCMv3.3.1 (based on: Barone et al. (1995))



2.2.2 The addition of the isomerization branch

Following the discovery of HPMTF (Veres et al., 2020) the pathway forming this molecule has now been well established (Wu et al., 2015; Veres et al., 2020; Berndt et al., 2019; Ye et al., 2021). The reactions of the isomerization branch that were added to CS2 (summarised in **Figure 1** and **Table 3**) were identified as those most important in determining SO₂ and HPMTF concentrations through sensitivity studies conducted using our box model setup. Details of these box model sensitivity studies (and the discarded reaction pathways that were found to not be significant) are included in the supplement. In this sense, species like HOOCH₂SCH₂OOH, included in the studies by Khan et al. (2021) were neglected from our mechanism as this was found to have minor impact on the SO₂ and HPMTF simulated in the box model experiments. The reactions that were added include the autoxidation of MTMP to HPMTF in one step (reaction 2ed) and the oxidation of HPMTF by OH, forming OCS (reaction 13b) and HOOCH₂S (reaction 13a) with further oxidation to SO₂ (reactions 14-16). The equilibrium with the O₂-adduct, HOOCH₂SOO, and its subsequent decomposition (reaction 14c, 15a,b) was included with kinetics equivalent to CH₃SOO (reaction 5c, 6a,b). Photolysis was found to be a minor pathway of HPMTF loss in our marine boundary layer box model setup (< 10%) and was omitted from the final mechanism used here; contrary to the importance of photolysis of HPMTF found by Khan et al. (2021).

Dry deposition of HPMTF is set using the same parameters in UKCA as other soluble gas-phase compounds, such as CH₃OOH and H₂O₂, which yield an average deposition velocity similar to the observations of Vermeuel et al. (2020) of 0.75 cm s⁻¹. For wet deposition of HPMTF, the Henry's law coefficient calculated by Wollesen de Jonge et al. (2021) was used.

For the sensitivity runs described in **Table 1**, some changes are made to the values in **Table 3**. In DMS-HPMTF-FP, the rate constant of reaction 2d is scaled by a factor of 5.0: Berndt et al. (2019) experimentally determined the rate constant at 295 K as 0.23 s⁻¹. Here the A-factor is scaled to match this value, while keeping the temperature dependence calculated by Veres et al. (2020) (following Wollesen de Jonge et al. (2021)). DMS-HPMTF-FL uses a rate constant 5.5 times faster for the total loss of HPMTF to OH (reaction 13a,b), which was recommended as an upper bound by Vermeuel et al. (2020) and following Khan et al. (2021). This range, between the base rate constant and the faster loss, puts us in the middle of the value experimentally determined by Ye et al. (2022). In the remaining sensitivity run CS2-HPMTF-CLD, heterogeneous uptake to both clouds and aerosols was added with reactive uptake coefficient (γ) of 0.01 (following Novak et al., 2021).

Table 3: Summary of the isomerization branch of the H-abstraction pathway. Rate constants referenced to this work are described in Section 2.2

Development and intercomparison of DMS oxidation mechanisms

No.	Reaction	Rate (cm ³ molecule ⁻¹ s ⁻¹)	Reference
2d	MTMP → HPMTF + OH	see note ^a	Veres et al. (2020)
13a	HPMTF + OH → HOOCH ₂ S + H ₂ O + CO	1.0×10 ⁻¹¹ × 0.9	this work
13b	HPMTF + OH → OCS + OH + HCHO + H ₂ O	1.0×10 ⁻¹¹ × 0.1	this work
14a	HOOCH ₂ S + O ₃ → HOOCH ₂ SO	1.15×10 ⁻¹² exp ^(430/T)	Wu et al. (2015)
14b	HOOCH ₂ S + NO ₂ → HOOCH ₂ SO + NO	6.00×10 ⁻¹¹ exp ^(240/T)	Wu et al. (2015)
14c	HOOCH ₂ S + O ₂ → HOOCH ₂ SOO	1.20×10 ⁻¹⁶ exp ^(1580/T) × [O ₂]	this work
15a	HOOCH ₂ SOO → HOOCH ₂ S + O ₂	3.50×10 ⁺¹⁰ exp ^(-3560/T)	this work
15b	HOOCH ₂ SOO → HCHO + OH + SO ₂	5.60×10 ⁻¹⁶ exp ^(-10870/T)	this work
16a	HOOCH ₂ SO + O ₃ → HCHO + OH + SO ₂	4×10 ⁻¹³	Wu et al. (2015)
16b	HOOCH ₂ SO + NO ₂ → HCHO + OH + NO + SO ₂	1.2×10 ⁻¹¹	Wu et al. (2015)

316 ^a 2.24×10⁺¹¹ exp^(-9800/T) exp^{(1.03e8/(T×T×T))}

317

318 2.3 Description of observational data

319 2.3.1 The NASA Atmospheric Tomography (ATom) mission

320 An observational dataset used to compare with the model simulations stems from the fourth flight campaign of the NASA
 321 Atmospheric Tomography mission (ATom-4). ATom-4 took place during April and May 2018, and completed a global circuit
 322 around the Americas: from the Arctic to the Antarctic over the remote Pacific and Atlantic Ocean at varying altitudes up to 12
 323 km. A vast number of atmospheric species were measured, including DMS, HPMTF, and SO₂ (Wofsy et al., 2018).

324

325 In order to compare the 3D model outputs with the data from the ATom-4 campaign, the hourly outputs from the respective
 326 model runs were interpolated in regards to time and space to generate the data along the flight path. Only model data at times
 327 where valid atmospheric measurements were available are taken into account, resulting in 313 data points for DMS (Whole
 328 Air Sampling) and 36,652 for SO₂ (Laser Induced Fluorescence).

329

330 2.3.2 Surface observations

331 Other observational measurements are monthly averages (mean) from the years 1990 to 1999 for DMS measurements made
 332 on Amsterdam Island (37°S, 77°E) in the southern Indian Ocean (Sciare et al., 2000) and the monthly means from 1991 to
 333 1995 for sulfate at the Dumont d'Urville station (66°S, 140°E) at the coast of Antarctica (Minikin et al., 1998). The diel profile
 334 of HPMTF as measured at Scripps Pier in July 2018 was taken from Vermeuel et al. (2020). [See the SI for the analysis of the](#)
 335 [modelled and observed DMS mixing ratios.](#)

3 Comparison of DMS oxidation pathways (BOXMOX)

Here we present the results of a series of box model simulations using the BOXMOX model (Weber et al., 2020). With BOXMOX we look at the diversity in results from simulations using a range of mechanisms, including our newly developed mechanism. These simulations are not constrained to observations or simulation chamber data. The set-up of the BOXMOX simulations is described in Section 2.1.1. We focus the analysis here on DMS and its major oxidation products and the effects of temperature and $[\text{NO}_x]$ on these. Section 3.1 compares DMS mechanisms based around the CS2 and ST schemes used in UKCA (Table 1). In Section 3.2 our newly developed mechanism is compared to other DMS mechanisms from recent literature that also include HPMTF formation.

3.1 Comparison of DMS mechanisms used for UKCA

3.1.1 Time series analysis

The BOXMOX set up allows a quasi steady-state to be achieved for a number of key sulfur species with the main exception being H_2SO_4 , which builds up over time in the model as the model is run without aerosol formation and aerosol microphysics included (Figure 2). The DMS concentration simulated with different DMS mechanisms used in UKCA is simulated to be very similar throughout all model runs; the small variations stem from different oxidant concentrations or small differences in the rate constants used for the initiation reaction in the different mechanisms (Figure 2a). For instance, the ST run has higher DMS concentration because the NO_x concentration is lower (as is OH) and less DMS is oxidised.

The SO_2 concentration is increased and MSA is significantly decreased in the updated CS2 runs (CS2-HPMTF and CS2-UPD-DMS) compared to CS2 (Figure 2b,c). Comparing CS2-HPMTF and CS2-UPD-DMS, we can see that this pattern (increased SO_2 and decreased MSA) is due to reaction 7c, which directly forms SO_2 and suppresses CH_3SO_2 , consequently lowering MSA formation. The SO_2 concentration is lower in CS2-HPMTF compared to CS2-UPD-DMS because the addition of HPMTF produces OCS which acts as a long-lived sulfur reservoir. While MSA concentration is very similar between CS2 and ST, SO_2 concentration is not. This is primarily explained through the difference in the treatment of MSA and SO_2 production in CS2 and ST. MSA is not treated as a reactive species in CS2 and ST (in so much as there are no further reactions of MSA after its production). In ST and ST-CS2, 100% of DMS yields SO_2 , regardless of the amount of MSA production. However, as more MSA is produced in CS2 the SO_2 yield is lowered. In spite of higher SO_2 concentrations in the ST DMS schemes, this trend does not translate to H_2SO_4 concentration (Figure 2d). SO_2 is a relatively long-lived species (~2 days in our model but with a range from 0.5-2.5 days (Lee et al., (2011))) and can therefore be lost through the mixing processes with the background air in the BOXMOX setup. In CS2, CH_3SO_3 decomposition provides a direct pathway to H_2SO_4 production. In the updated CS2 schemes (CS2-UPD-DMS and CS2-HPMTF) SO_3 production with instantaneous transformation to H_2SO_4 is included. The slower rate constant in CS2 for the decomposition of CH_3SO_3 (11b_old) is compensated by a higher production of CH_3SO_3 .

Formatted: Subscript

Development and intercomparison of DMS oxidation mechanisms

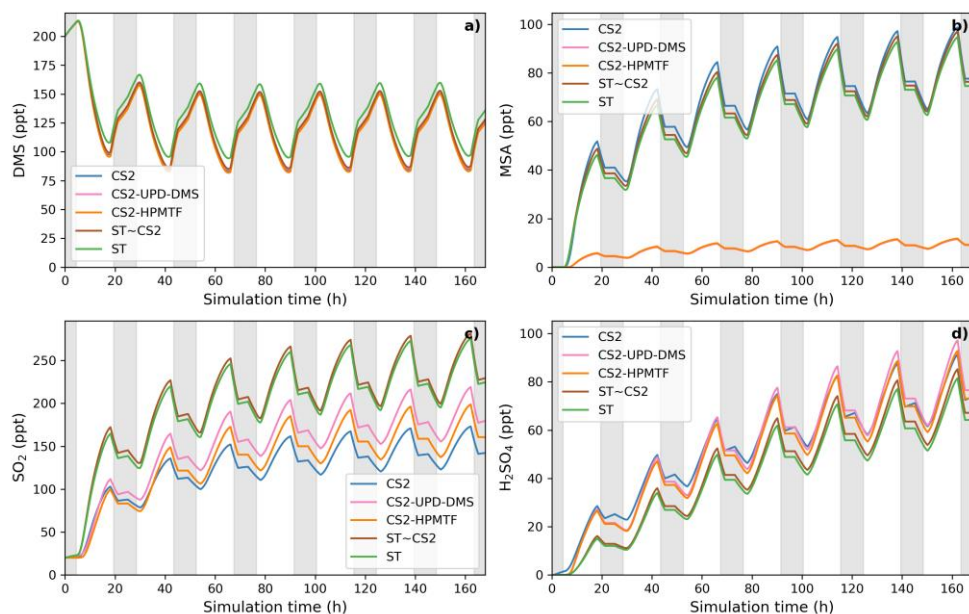


Figure 2: BOXMOX-simulated gas-phase concentrations as a function of time for a selection of species simulated with the different DMS gas-phase oxidation schemes used in UKCA configurations (oxidation by OH and NO₃). Grey areas denote nighttime, when no photolysis reactions are taking place. Average NO_x concentration is approximately 10 ppt, with an average temperature of 293 K (range: 289 – 297 K).

3.1.2 Sensitivity of UKCA DMS schemes to temperature

As described in Section 2.1.1, a series of BOXMOX experiments were performed perturbing the temperature profile in the model (Figure 3).

As temperature increases in the box model, the steady-state DMS concentration increases in all simulations. This is mainly because the DMS oxidation by OH addition is negatively temperature dependent. For most models, DMS concentration increases by 85-93 ppt throughout the temperature range from 260 K to 310 K, except the ST run where at temperatures over 290 K, a stronger increase of DMS concentration is found, with a total increase of 106 ppt. This could be due to different

Development and intercomparison of DMS oxidation mechanisms

oxidant concentrations in the model runs using the ST mechanism and independent of the DMS scheme since this stronger increase is not found with CS2-ST.

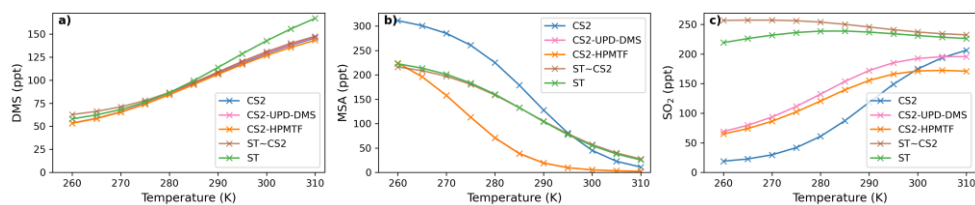
Although the kinetics, and therefore temperature dependence, of DMS loss is comparable across the different schemes, the dependence of MSA and SO₂ on temperature differ significantly.

Most MSA is formed from the OH-addition channel, which is favoured at low temperatures (Barnes et al., 2006). Therefore, the MSA concentration is higher at lower temperatures across all the UKCA DMS schemes considered (**Figure 3b**). In the ST schemes (ST and ST~CS2), MSA decreases by around 88% (-189 ppt and -197 ppt) throughout the temperature range considered, while in all the CS2 schemes MSA is shown to be much more sensitive to temperature, decreasing by >96% (CS2: -300 ppt, CS2-UPD-DMS: -222 ppt, CS2-HPMTF: -222 ppt). In particular the CS2 family of mechanisms shows pronounced temperature sensitivity between 270 to 290 K. We attribute this to differences in the rate constant of DMS oxidation through the OH-addition channel (see **Table 2** and **S1.3.1**). The average MSA concentration for the UKCA schemes diverges most in the temperature range between 270 - 300 K.

The difference in SO₂ concentrations between the CS2 schemes and ST schemes are greatest at lower temperature (**Figure 3c**), with the ST and CS2-ST schemes simulating ~ 5 times (+200 ppt) the SO₂ that is simulated in the other schemes based around CS2. In the ST schemes SO₂ concentration either stays at a similar level across the whole temperature range (ST: +3%) or slightly decreases (ST~CS2: -9%). Conversely, the CS2 family of schemes show a positive temperature dependence (i.e., $+\frac{d[X]}{dT}$), across the temperature range, especially in the range of relevant atmospheric temperatures from 270 to 290 K. SO₂ increases by 298% in CS2, 84% in CS2-UPD-DMS and 79% CS2-HPMTF. In the CS2 schemes, more DMS reacts through the addition pathway which favours the production of MSA, instead of SO₂ therefore reducing the SO₂ concentration. In ST, the addition pathway still leads to 100% SO₂ formation, making the average SO₂ concentration less dependent on temperature. Experimental findings (Arsene et al., 1999) and field measurements (Sciare et al., 2001) both show a positive temperature dependence of SO₂ concentration. This trend is only reproduced by the DMS schemes based on the CS2 mechanistic features (i.e. not the very simple mechanism used in ST), indicating that the ST DMS chemistry is likely insufficient to explain laboratory and field observations, particularly in cold environments and under climate change.

In these box model experiments only gas phase losses and mixing of species with background air are considered. Under the conditions of our simulations, we find that the MTMP isomerization pathway mainly yields SO₂, as does the rest of the abstraction pathway. Therefore, the addition of the isomerization branch does not have a significant impact on the temperature dependence of SO₂ concentration (comparing CS2-UPD-DMS and CS2-HPMTF), even though the isomerization step itself is greatly temperature dependent.

Development and intercomparison of DMS oxidation mechanisms



412
413 **Figure 3:** Temperature dependence of average a) DMS, b) MSA, and c) SO₂ concentration after a quasi steady-state is reached
414 in the box model simulations using the DMS schemes for UKCA.
415

416 3.2 Comparison with DMS schemes that include HPMTF from the recent literature

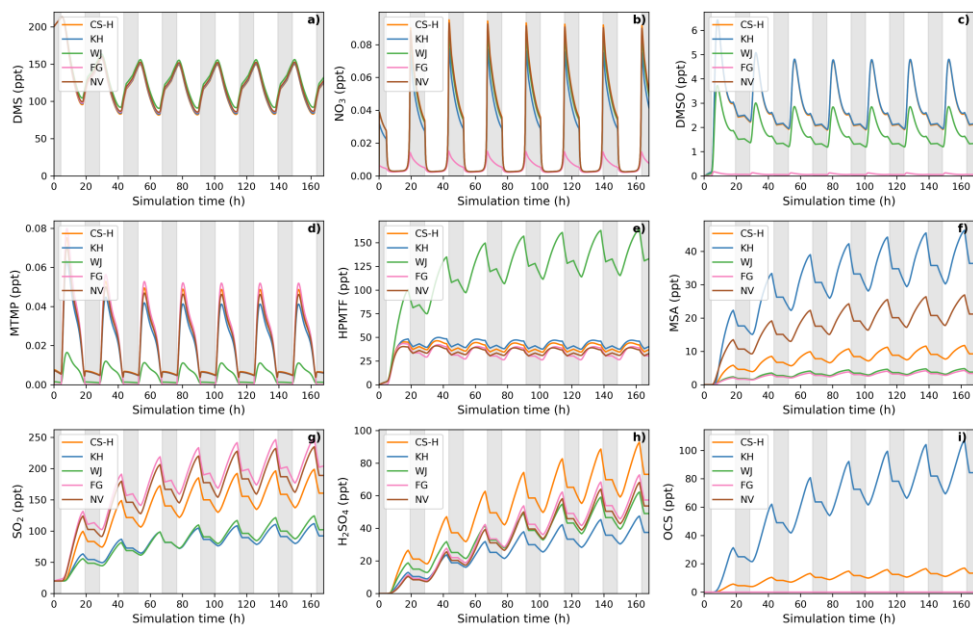
417 Here, four recently published DMS schemes that also include the isomerization pathway and formation of HPMTF are
418 compared with our new mechanism, CS2-HPMTF (*CS-H*, 36 reactions in DMS scheme), as follows. To make the studies
419 comparable, only DMS oxidation by NO₃ and OH and gas-phase reactions are considered. The implementation of these
420 chemical schemes in BOXMOX can be found in the *Supporting Information SI.3*.

- 421 • *Fung et al. (2022) (FG)*: This scheme includes 32 reactions for the DMS oxidation chemistry. The H-abstraction
422 pathway is based on the MCM, while the rate constants in the OH-addition pathway mostly stem from Burkholder et
423 al. (2015) or a scaled up version of those. The rate constant of MTMP isomerization to HPMTF is based on Veres et
424 al. (2020).
- 425 • *Wollesen de Jonge et al. (2021) (WJ)*: This scheme is the most complex and consists of 98 reactions, including
426 reactions from the MCM and from Hoffmann et al. (2016). The isomerization branch mostly uses the rate constants
427 by Wu et al. (2015), except the first isomerization rate constant, which is a combination of Veres et al. (2020) and
428 Berndt et al. (2019).
- 429 • *Khan et al. (2021) (KH)*: This scheme is based on Khan et al. (2016), which is equivalent to the DMS chemistry in
430 CS2 (CRI v2 R5). The mechanism was modified to include the isomerization pathway and photolysis loss and
431 temperature dependent OH oxidation of HPMTF by the authors. In total, the DMS chemistry consists of 38 reactions,
432 5 of which are photolysis reactions.
- 433 • *Novak et al. (2021) (NV)*: This is a simplified scheme that aims to only include the intermediates necessary for
434 HPMTF formation and consists of only 10 reactions. DMS therefore either directly yields MSA (without DMSO
435 formation) or first forms MTMP, which isomerizes to form HPMTF or is oxidised to SO₂.
436

Development and intercomparison of DMS oxidation mechanisms

437 Using this ensemble of gas-phase DMS oxidation schemes in BOXMOX simulations leads to significant differences in the
438 concentrations of important oxidation intermediates and products, even though DMS concentration is similar across all models
439 (Figure 4).

440 3.2.1 Time series analysis of different DMS-HPMTF schemes



441
442 **Figure 4:** Gas-phase concentrations as a function of time for different DMS gas-phase oxidation schemes (oxidation by OH
443 and NO₃). Average NO_x concentration is approximately 10 ppt, with an average temperature of 293 K (range: 289 – 297 K).
444 Grey areas denote nighttime when no photolysis reactions are taking place.

445
446
447 The depletion of DMS due to OH and NO₃ oxidation is similar across most models (Figure 4a) since the major oxidants are
448 relatively constrained by the box model experiment set up (see Section 2.1.1) and they mostly rely on IUPAC or JPL
449 recommended values (Atkinson et al., 2004; Burkholder et al., 2015). One exception is the NO₃ oxidation in the FG scheme,
450 which uses a rate constant is a factor of approximately 6 higher than the JPL rate constant recommendation. On the one hand,
451 this does not affect DMS concentration, since OH oxidation of DMS plays a greater role, on the other hand, the concentration

Development and intercomparison of DMS oxidation mechanisms

of NO_3 in the FG scheme's simulation run is controlled by the greater NO_3 oxidation rate (**Figure 4b**). WJ includes the intermediate $\text{CH}_3\text{S}(\text{OH})\text{CH}_3$ and its decomposition back to DMS (based on Hoffmann et al., (2016)), which in their experiments improved the fit between their measured and modelled DMS concentration. Here, this does not have any significant impact on DMS concentration, compared to all the other schemes.

Significant differences between the models can be found for the DMSO concentration (**Figure 4c**). KH and CS-H have the highest DMSO concentration since all DMS that is oxidised through the OH-addition pathway yields DMSO. This is not the case for WJ, where CH_3SOH and to a small part DMSO_2 are also possible products. In the FG simulation, DMSO concentration is close to zero, which is due to a much faster loss of DMSO; a rate constant a factor of 15 faster than experimental measurements by Urbanski et al. (1998). NV does not include DMSO as an intermediate. Since the lifetime of DMSO was found to be several hours (Urbanski et al., 1998; Ye et al. 2021), deposition of DMSO could act as a significant sink of atmospheric sulfur (as found by Chen et al. (2018)). Fast oxidation of DMSO in FG, or omitting the species in NV, might therefore lead to an over-estimation of other DMS oxidation products in those schemes.

Regarding the intermediate MTMP, WJ shows the greatest deviation from the ensemble (**Figure 4d**). The MTMP concentration never exceeds 0.02 ppt in WJ, while the other mechanisms simulate concentrations over three times higher. WJ employs a faster isomerization rate constant of MTMP to HPMTF. They scale the A-factor by 5 to get a rate constant that is a combination of the theoretical calculations by Veres et al. (2020) and the experimental findings by Berndt et al. (2019). Additionally, they include more oxidation reactions of MTMP (such as oxidation by NO_3) but since the isomerization to HPMTF already outcompetes most oxidation reactions anyway (>97%), we found them to play a negligible role (<0.1%). In the FG scheme, $\text{DMS} + \text{NO}_3$ leads to immediate SO_2 formation, without prior MTMP formation. Therefore, no MTMP is produced during the nighttime, when NO_3 oxidation becomes relevant. Under conditions with low NO_x (around 10 ppt in this experiment) this does not have significant impacts but at higher NO_x concentrations this leads to a major deviation from the other simulations (**Figure 5a**, 100 ppt NO_x). At night, CS-H, KH, and NV reach MTMP concentrations of 0.07 ppt, allowing nighttime HPMTF formation, while FG stays zero.

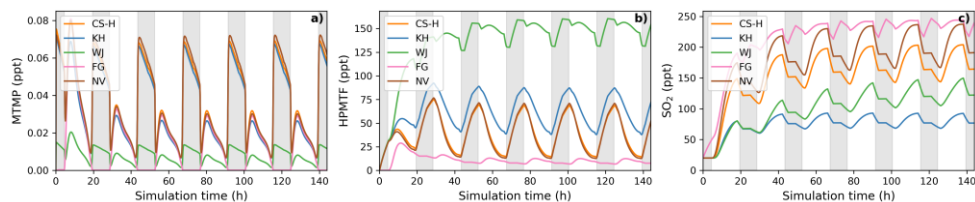
All model simulations, except WJ, are very similar in HPMTF concentration (**Figure 4e**). The fast isomerization rate constant in WJ is one of the reasons HPMTF concentration is on average more than 3 times higher than the other model simulations. The other reason is a much slower oxidation of HPMTF by OH. While most models use a value of (or close to) $1.11 \times 10^{-11} \text{ cm}^3 \text{ molecule}^{-1} \text{ s}^{-1}$, recommended by Vermeuel et al. (2020), WJ use the much slower rate constant calculated by Wu et al. (2015), $1.4 \times 10^{-12} \text{ cm}^3 \text{ molecule}^{-1} \text{ s}^{-1}$. This rate constant is also used in the KH scheme but it additionally includes HPMTF depletion by photolysis which ultimately leads to the similar HPMTF concentration as in CS-H, FG, and NV. The addition of the photolysis reactions in KH does not affect the diel profile of HPMTF, even though those account for 81% of chemical loss of HPMTF in their scheme. It is therefore unlikely that the observed diel profile of HPMTF by Vermeuel et al. (2020) and

Development and intercomparison of DMS oxidation mechanisms

486 Khan et al. (2021) can be explained solely by considering loss of HPMTF to aldehyde and hydroperoxide photolysis. Reducing
487 HPMTF formation to one isomerization reaction without any side reactions as is done in this work and NV, does also not affect
488 the diel profile of HPMTF significantly.

489 The effect of higher NO_x conditions on the diel profile of HPMTF varies significantly between the different schemes (10 ppt
490 NO_x in **Figure 4** vs. 100 ppt NO_x in **Figure 5**). Higher NO_x concentration leads to more DMS oxidation by NO₃ at night and
491 the subsequent increase in MTMP concentration and therefore HPMTF concentration during the night hours in the CS-H, WJ,
492 KH, and NV simulations. At low NO_x, HPMTF concentration stayed more or less stable throughout the nighttime and increased
493 in the morning, reaching a plateau in the afternoon, and dropping in the evening (**Figure 4e**). Under higher Nox conditions,
494 HPMTF increases in these mechanisms throughout the night and decreases throughout the day when it is oxidised by OH
495 (**Figure 5b**). In the WJ simulation, the diel profile has more plateaus and small deviations but the overall trend still fits the
496 described pattern. This is not true for FG, where DMS oxidation by NO₃ leads directly to SO₂ formation.

497



498

499 **Figure 5:** BOXMOX simulations where the average NO_x concentration is approximately 100 ppt (a factor 10 greater than for
500 the results presented in **Figure 4**). (a) MTMP, (b) HPMTF, and (c) SO₂ concentration as a function of time for different DMS
501 gas-phase oxidation schemes (oxidation by OH and NO₃). Average temperature of 293 K (range: 289 – 297 K). Grey areas
502 denote nighttime when no photolysis reactions are taking place.

503

504 While the diel profile of MSA looks similar for all simulations, the average concentrations do not (**Figure 4f**). The highest
505 average steady-state MSA concentration is reached in the KH simulation, which is a factor of 10 higher than the lowest average
506 concentration in the FG simulation. In our experimental setup, most of the simulations we performed with the different
507 mechanisms do not include any (significant) gas-phase chemical loss pathway for MSA; MSA is only lost through mixing and
508 transport out of the "box". Therefore, the concentration of MSA is a direct reflection of MSA production in the respective
509 simulations.

510

511 KH simulates the highest production of MSA (similar to CS2), where MSA is formed through the addition (MSIA + OH →
512 0.05 MSA + 0.95 CH₃SO₂, reaction 9b,c) and the abstraction channel (CH₃SO + O₃ → CH₃SO₂, reaction 7c_old) of DMS
513 oxidation, with CH₃SO₂ partly being oxidised to CH₃SO₃ and then to MSA (reactions 10b,c, 11a). The decomposition of

Development and intercomparison of DMS oxidation mechanisms

514 CH_3SO_3 to H_2SO_4 in KH is slower than in other mechanisms, increasing the branching ratio for MSA formation in their
515 mechanism. In NV, the simulation with the second highest average MSA concentration, the only source of MSA is the direct
516 production of MSA through OH oxidation through the addition channel, where 25% of DMS forms MSA. In both, CS-H and
517 WJ, the abstraction pathway mostly produces SO_2 and only contributes negligible amounts to CH_3SO_2 formation, hence MSA.
518 Similar to KH, the oxidation of DMS through the addition pathway in CS-H and WJ yields CH_3SO_2 of which a part forms
519 MSA. However, not all of the CH_3SO_2 results in MSA, some of it also decomposes to SO_2 or yields SO_3 . This explains the
520 lower concentration of MSA in CS-H and WJ compared with NV. The reason why CS-H has a higher MSA concentration than
521 WJ is because of the inclusion of reaction 9b (**Table 2**), which yields MSA directly and is not part of the WJ scheme.
522 The lowest MSA concentration is found in FG and WJ, where 60% of the OH-addition pathway directly produces SO_2 . Out of
523 the 40% of DMS that forms DMSO in this pathway, only a fraction yields MSA.

524
525 To harmonise the results and aid interpretability, the same rates (based on CS2) are used for the loss processes of SO_2 in all
526 the mechanisms considered here, therefore the concentration of SO_2 can be used as a proxy for SO_2 production, just as for
527 MSA. The highest SO_2 concentration can be seen in schemes that have the smallest number of intermediates or the most direct
528 pathways from DMS to SO_2 , in NV and FG (**Figure 4g**). Fewer intermediates result in less opportunities for the formation of
529 side products or less long-lived species that can be lost through transport or deposition. For instance, in WJ HPMTF is lost
530 through mixing with the background before it can form SO_2 . Likewise, KH has a higher ratio of MSA and OCS production,
531 which lowers the SO_2 yield. The diel profile of SO_2 concentration is in most simulations not affected by higher NO_x
532 concentrations, with the general trend being an increase of SO_2 concentration during the day and a decrease at night (**Figure**
533 **5c**). The only exception is the FG simulation, where we see a clear increase through part of the night, due to the reaction DMS
534 $+ \text{NO}_3 \rightarrow \text{SO}_2$.

535
536 The H_2SO_4 concentration is influenced by SO_2 production and CH_3SO_3 production and the rate of decomposition of SO_3 to
537 H_2SO_4 . CS-H has the highest average H_2SO_4 concentration and KH the lowest; all other models are very similar to each other
538 (**Figure 4h**). In general, higher SO_2 concentration leads to more H_2SO_4 , since SO_2 is first oxidised to SO_3 and then to H_2SO_4
539 with the same rates across all schemes. However, all models except NV include an additional pathway of H_2SO_4 formation: in
540 KH and FG, H_2SO_4 is directly formed from CH_3SO_3 , while in CS-H and WJ CH_3SO_3 decomposes to SO_3 first, which then
541 instantly reacts to H_2SO_4 . In KH, the rate constant for the decomposition of CH_3SO_3 at 295 K is a factor of 15 slower than in
542 the other models. Since the SO_2 concentration is also relatively low, it explains why KH has the lowest H_2SO_4 concentration
543 of all schemes when reaching steady-state. CS-H results in a higher H_2SO_4 concentration than FG or NV even though those
544 models have a higher SO_2 concentration. The reason is a higher production of CH_3SO_3 that is then decomposed to SO_3 and
545 H_2SO_4 .

546

Development and intercomparison of DMS oxidation mechanisms

547 Similar to the other products of the DMS scheme, the concentration of OCS is a reflection of its production. OCS is only
548 produced from oxidation of HPMTF by OH and, in the KH scheme, through photolysis of HPMTF. In KH, 60% of HPMTF
549 forms OCS, resulting in the highest OCS concentration (**Figure 4i**). This stems mainly from the large contribution of the
550 photolysis reactions. Potentially, the rate constant of OH oxidation of HPMTF in KH is too low and therefore OCS might be
551 overestimated. In CS-H, 10% of HPMTF is oxidised to OCS, resulting in an OCS concentration that is on average 5.5 times
552 lower than KH. FG and WJ both use the theoretically determined branching ratio by Wu et al. (2020), which results in only
553 0.007% of HPMTF being oxidised to OCS at 295 K. NV does not include this pathway. Very recent evidence suggests that
554 there is a small (2%) but prompt source of OCS following the formation (and decomposition) of HPMTF as well as a significant
555 OCS yield (13%) from the HPMTF + OH reaction (Jernigan et al., 2022). These new data were not assessed (or included) in
556 this work but we estimate that inclusion of these mechanistic pathways would result in OCS yields ~~between-higher than~~ CS-H
557 and the other mechanisms (which have used a very small yield in the past) ~~i.e.but~~ consistently lower than that simulated by
558 KH.

559 To summarise, the intercomparison of recent gas-phase DMS oxidation mechanisms complements and extends earlier studies
560 on DMS (Karl et al., 2007). Recent gas-phase DMS oxidation schemes used in modelling studies lead to a wide range in results
561 of key DMS oxidation products, with moderate Nox levels (~ 0.1 ppb) leading to greater divergence than low Nox levels (~
562 10 of ppt). A similar situation was found for isoprene by Archibald et al. (2010) and significant efforts have been employed to
563 improve our understanding of isoprene oxidation through theoretical and laboratory experiments (e.g., Jenkin et al., 2015;
564 Wennberg et al., 2018). We now focus on the role of temperature on the divergences seen thus far.

3.2.2 Temperature dependence of different DMS-HPMTF schemes

567 **Figure 6** shows that even though the temperature dependence of average DMS concentration is similar across all schemes, the
568 temperature dependence of average SO₂ and MSA concentration differs from scheme to scheme significantly. Most of the
569 general trends were found to be similar and in line with the trends observed for the UKCA schemes and have been explained
570 there (Section 3.1.2, **Figure 3**).

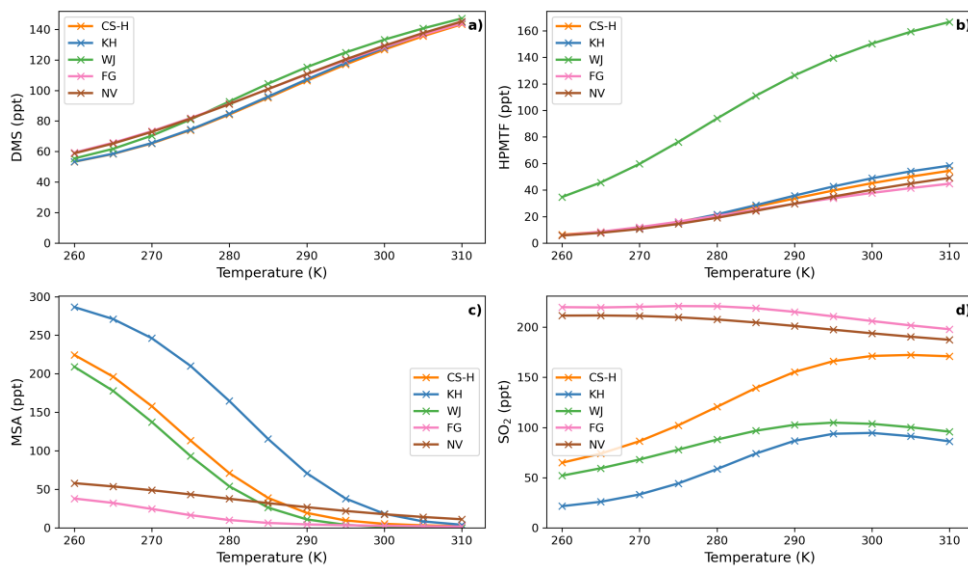
571
572 While WJ has the highest absolute change in HPMTF concentration throughout the temperature range (+131 ppt, +380%;
573 **Figure 6b**), CS-H, KH, and NV show higher relative change (+43-48 pp, +763-892%). Since FG is missing the DMS oxidation
574 by NO₃ as a potential pathway to HPMTF (via MTMP), HPMTF in FG is least affected by temperature (+34 ppt, +256%).

575
576 MSA is even more affected by temperature than HPMTF (**Figure 6c**). Its concentration shows a strong negative temperature
577 dependence in all simulations (**Figure 6c**). The magnitude of MSA-temperature dependence differs from scheme to scheme.
578 The smallest changes can be observed in NV (-47 ppt from 260 – 310 K), where only 25% of DMS that is oxidised through
579 the OH-addition pathway forms MSA. Similarly in FG (-67 ppt from 260 – 310 K), where only 40% of the OH-addition

Development and intercomparison of DMS oxidation mechanisms

580 pathway forms DMSO and then potentially MSA. The largest temperature dependence can be found in the KH simulation,
 581 with a change of MSA concentration of -282 ppt from 260 K to 310 K, which is very similar to CS2 (Figure 3c).

582
 583 In almost all schemes, SO₂ concentration increases with temperature (Figure 6d). The greatest positive change happens
 584 between the atmospheric relevant temperatures 270 and 290 K. KH and CS-H show the greatest increase in this temperature
 585 range with +53 ppt (+160%) and +69 ppt (+80%), respectively (WJ: +34 ppt (51%)). Starting at 295 K, SO₂ concentration
 586 plateaus with further increasing temperature and even declines slightly in some simulations (Figure 6d). NV and FG are the
 587 only models which show a decrease in SO₂ throughout the entire temperature range of 260 – 310 K (NV: -24 ppt, -11%, FG:
 588 -22 ppt, -10%), similar to ST-CS2 in Figure 2d. This could be due to previously mentioned simplifications in the DMS
 589 additional channel, where DMSO is either completely omitted or rapidly oxidised further.



591
 592 **Figure 6:** Temperature dependence of average (a) DMS, (b) HPMTF, (c) MSA, and (d) SO₂ concentration in different DMS
 593 oxidation schemes after a quasi steady-state is reached in the box model simulation. Average No_x is approximately 10 ppt.

594
 595 These results demonstrate limited consensus on gas-phase DMS oxidation, similar to the earlier work of Karl et al., 2007.
 596 Importantly in the context of the role of DMS in chemistry-aerosol-climate feedbacks, we have further shown that this

Development and intercomparison of DMS oxidation mechanisms

597 uncertainty across mechanisms is amplified when assessing temperature sensitivity of the products of DMS oxidation. Small
598 uncertainties in the rate of reactions or the omission of intermediates can have significant effects on the resulting product
599 concentrations, [as we have shown through our systematic work updating the CRI-Strat DMS scheme. All models studied tend](#)
600 [to agree on the rates of oxidation of DMS, largely controlled for by the fairly uniform treatment of the initial oxidation step.](#)
601 [However, we saw \(in Figure 5\) that there is large divergence at high Nox levels for MTMP and subsequently HPMTF and](#)
602 [SO₂. In part this divergence could be reduced by better constraining the MTMP self- and cross-reactions, but in the case of](#)
603 [Fung et al. \(2022\) including MTMP as a product of the NO₂ + DMS reaction would help it converge with the other models.](#)
604 [The effects of climate change are that it is likely that global mean surface temperature will remain higher than the pre-industrial](#)
605 [baseline for some time to come. As a result, the simulations would all suggest an increase in the amount of HPMTF formed](#)
606 [relative to other major oxidation products, especially, MSA, and most likely an overall increase in SO₂. However, our box-](#)
607 [modelling study highlights how uncertain the situation is within the context of the current literature.](#) At present there is a need
608 for more laboratory data and more focused sensitivity studies to isolate the major sources of uncertainty that are common
609 across DMS oxidation mechanisms and constrain them. Strikingly we see that the ST and CS2 mechanistic variants used for
610 UKCA studies span the wide range of SO₂-Temperature and MSA-Temperature sensitivities as the recently reported updated
611 DMS mechanisms. We now move on to discuss our work implementing the CS2-H mechanism into our global chemistry-
612 climate model.

Formatted: Subscript

Formatted: Subscript

Formatted: Subscript

Formatted: Subscript

613 4 Results from 3D model simulations using UKCA

614 Here we present our results from the incorporation of the new CS2-H DMS mechanism described above in the 3D UKCA
615 chemistry climate model. As described in Section 2.1, we performed a series of ~~12-month~~12-month nudged simulations with
616 UKCA for the year 2018 using 6 model simulations, with different mechanistic variants (**Table 1**). As a reminder, we use the
617 CS2 simulation (Archer-Nicholls et al., 2021) as the “base” simulation, to which mechanistic improvements are made. [More](#)
618 [details can be found in the SI in Section 2.](#)

619 4.1 Distribution of **key sulfur species (DMS, HPMTF, SO₂ and sulfate).**

Formatted: Subscript

620 The annual mean global DMS burden was found to be between 63-66 Gg S in all model simulations. DMS concentration
621 follows a seasonal modulation with maximums in the warmer months, which coincide with phytoplankton blooms (**Fig. 7a**).
622 **Figure 7b** and **7c** show the annual mean vertical profiles in the central North Atlantic region and the Southern Ocean (see
623 figure caption for bounding areas). These regions are focused on owing to the differences shown in the mixing ratios of key
624 species and the importance of these two regions to global climate (e.g., Sutton et al., 2018; Caldeira and Duffy 2000). In the
625 Southern Ocean, DMS mixing ratios vary between 100 and >300 ppt. On the other hand, in the North Atlantic region analysed,
626 DMS concentrations rarely reach over 50 ppt. Here, <1 ppt DMS is found above the boundary layer (above 1000 m), while in
627 the Southern Ocean DMS decreases more slowly up-to the tropopause (~8000 m). These differences in DMS distribution are

Development and intercomparison of DMS oxidation mechanisms

a complex function of the local heterogeneity of the DMS source from the ocean and differences in the lifetime of DMS due to different simulated cloud and oxidising environments (with the North Atlantic generally being a region of greater oxidising capacity than the Southern Ocean (Archer-Nicholls et al., 2021; Griffiths et al., 2021))

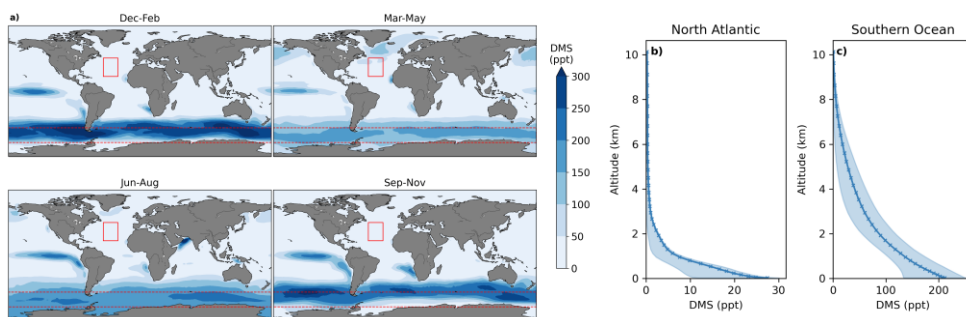


Figure 7: a) Global distribution of DMS mixing ratios in the lower troposphere (< 2 km) over the oceans in CS2. Annual mean vertical distribution of DMS in b) the Central North Atlantic (30-50°E, 20-45°N, denoted with the red rectangle in panel a) and in c) the Southern Ocean (50-70°S, denoted with the red dashed rectangle in panel a). The envelopes represent the interquartile range of the model simulation results. Note the order of magnitude difference in the DMS concentrations between the North Atlantic and Southern Ocean.

There is a significant bias in the simulated DMS mixing ratios compared with observations, which we note has been seen in several other modelling studies (e.g., Fung et al. (2022)) and is driven not by the DMS chemistry but by the oceanic emissions, in our case by the bias in the UKESM derived DMS emissions field (Bhatti et al., 2023). See the SI for further details.

4.1.1 Comparison of DMS with observations

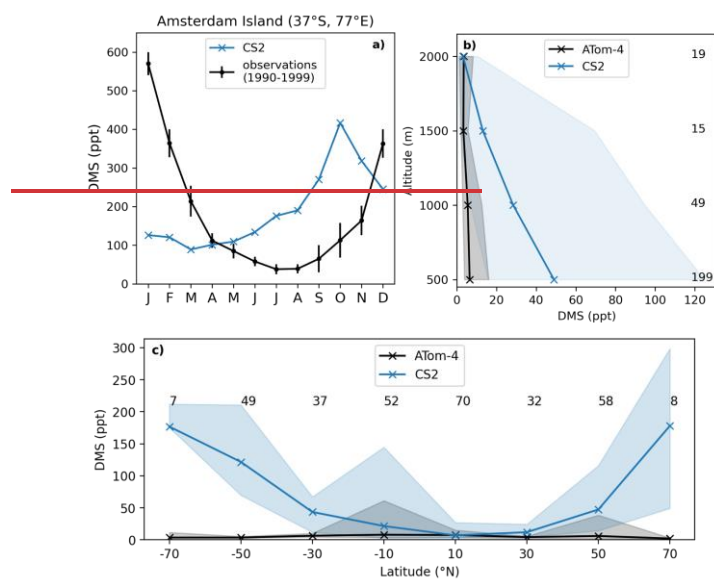


Figure 8: (a) Comparison of DMS surface concentration on Amsterdam Island (37°S, 77°E) in the southern Indian Ocean. The observational data (Sciare et al., 2000) represents the monthly mean concentrations and their standard deviations for the years 1990–1999. (b) Vertically binned (500 m) and (c) latitudinally binned (20°) median DMS mixing ratio along the ATom-4 flight path. The envelopes represent the interquartile range of the measurements and the respective model results while the numbers on the side/on top give the number of measurements in the respective bin. In b) and c) the model data are sampled along the ATom flight track using hourly mean model data.

DMS was not significantly affected by the different DMS mechanisms in the simulations with UKCA and so we focus on the results from the CS2 simulation. **Figure 8** compares observed DMS from ground-based measurements on the Amsterdam Island and *in-situ* measurements from the ATom-4 flights with the simulated DMS in CS2. On Amsterdam Island, a clear seasonality was observed for the monthly mean DMS concentration, with a peak during the austral summer (570 ppt) and a minimum during the austral winter (38 ppt). The simulated DMS (89–416 ppt) falls within that range but fails to capture the observed seasonal trends (**Figure 8a**). We suggest that the disagreement between the observed and modelled atmospheric DMS mixing ratios is driven by the DMS emissions dataset we have applied in this study. Boek et al. (2021) reviewed CMIP6 DMS

Development and intercomparison of DMS oxidation mechanisms

emissions and found that the emissions used in our study (from the UKESM-1 model) tend to result in less spatial heterogeneity than observational based climatologies (e.g., Lana et al. (2011)). During the tuning of the UKESM-1 model (Sellar et al., 2019) the DMS emission scheme was modified to have a minimum DMS ocean concentration of 1nM imposed, the effect of which seems to be to generally overestimate the DMS emissions over the low productivity regions. Overall, we found the atmospheric DMS concentration in the model (which hitherto has not been evaluated before) to be significantly higher compared with the airborne observations from ATom-4 (Figure 8b and c). At the altitudes shown, the model predicts DMS approximately 5 times higher than the measurements. A comparison along the latitudinal axis (Figure 8c) reveals that DMS is significantly overestimated at high latitudes (however, it should be taken into account that only few measurements exist for latitudes above 60° from ATom4).

It is difficult to evaluate atmospheric DMS globally as there are limited observations that can be used for evaluating global models. For instance, Amsterdam Island being one of only a handful of long-term observational sites, no remote sensing based data and with most atmospheric observations made on ships that are focusing on plumes of DMS. None the less, our CS2 base run (and all subsequent UKCA runs) suffer from a high bias in simulated atmospheric DMS, driven by the use of the emissions dataset we used. We opted to use the default UKESM DMS emissions as our focus in this study is the oxidation mechanism. However, we suggest that future work assess the impacts of both DMS emissions and chemistry using some of the more recent DMS emissions datasets (Gali et al., 2018; Hulswar et al., 2022). Bearing the caveats of DMS in mind, we now look at the intermediates and products of DMS oxidation.

4.1.12 Oxidation of DMS

We calculate a global average tropospheric lifetime of 1.5 days for DMS. Figure 89 shows the global distribution of the different DMS oxidation pathways in the base run (these results are not affected by the different DMS mechanism variants we use as these reactions were not updated and there is only a weak feedback of DMS oxidation products on DMS oxidation itself). 75% of DMS is oxidised by OH (41% via the OH-addition channel and 34% via the H-abstraction channel) and 25% by NO₃. Oxidation by NO₃ is dominant in the Northern Hemisphere, especially close to the coast and over ship routes. In the Southern Hemisphere, where DMS emissions are highest, the contribution is less than 20%. The addition pathway of OH oxidation is favoured at lower temperatures, explaining the trend of higher DMSO formation at high latitudes.

Development and intercomparison of DMS oxidation mechanisms

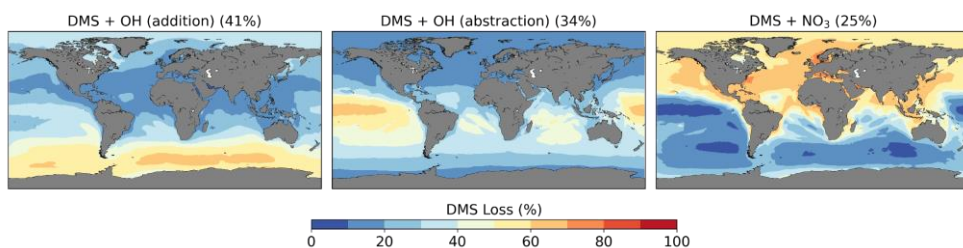
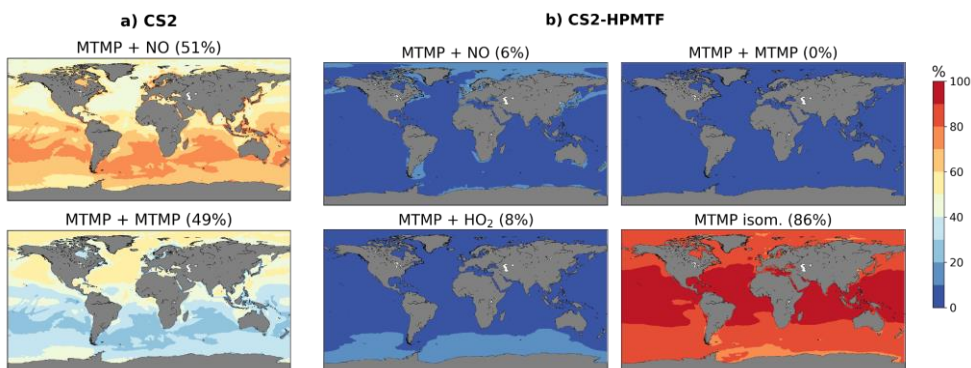


Figure 89: Spatial distribution of mean percentage of DMS oxidation via DMS + OH (addition), DMS + OH (abstraction), and DMS + NO₃ in the CS2 base run. The percentage in brackets denotes the contribution of this channel to the global chemical loss of DMS. Only values above the ocean are shown.

4.2 DMS Oxidation products

59% of DMS forms MTMP, the first intermediate of the abstraction pathway. In CS2, MTMP is oxidised by NO (51%) or reacts with itself (49%) to form CH₃S (Figure 190a) which is further oxidised to SO₂, H₂SO₄, and MSA. This is clearly wrong and a failure of the CS2 scheme. With the updates implemented in CS2-HPMTF, 86% of MTMP isomerizes to HPMTF, while 8% is oxidised by HO₂, and only 6% by NO (Figure 190b). The self-reaction becomes negligible with the additional loss processes of MTMP, significantly lowering MTMP concentrations. The global tropospheric lifetime of MTMP is reduced from 26 min to less than one minute.



Development and intercomparison of DMS oxidation mechanisms

Figure 910: Spatial distribution of annual mean percentage of MTMP depletion (< 2 km) via MTMP + NO, its self-reaction, MTMP + HO₂, and isomerization to HPMTF in **a)** CS2 and **b)** CS2-HPMTF. The percentage in brackets denotes the contribution of this channel to the global chemical loss of MTMP. Only values above the ocean are shown.

4.2.1 Modelled HPMTF

In CS2-HPMTF 51% of DMS forms HPMTF. The general patterns of the global distribution of HPMTF are similar to those of DMS in **Figure 140**, except that relatively higher concentrations of DMS are reached in the Southern Ocean. There, temperatures are lower and therefore the OH-abstraction pathway, as well as the strongly temperature-dependent isomerization reaction from MTMP to HPMTF are disfavoured. At the surface, the annual mean HPMTF concentration is similar in the North Atlantic and the Southern Ocean with approximately 20 ppt. However, in the North Atlantic, the variability throughout space and time is greater (bigger interquartile range). Further, the vertical profiles differ visibly: In the North Atlantic HPMTF concentration decreases in the boundary layer and above 2500 m HPMTF concentration is virtually zero (**Figure 140b**). In the Southern Ocean, the concentration decreases more slowly and only reaches zero at 10000 m (**Figure 140c**). The HPMTF burden in CS2-HPMTF is 24 Gg S and HPMTF has a lifetime of 26 hours

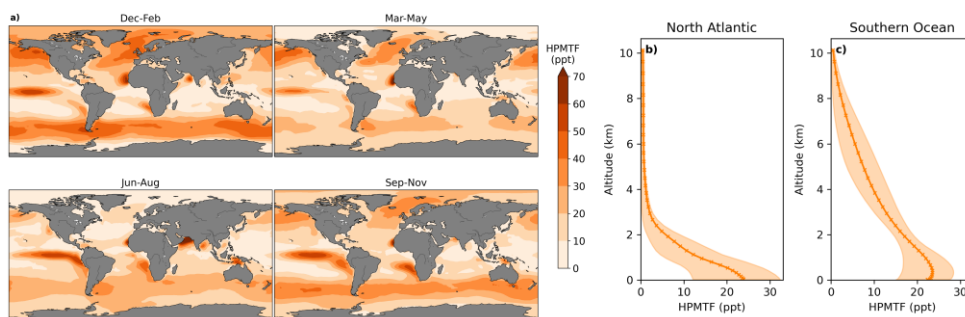


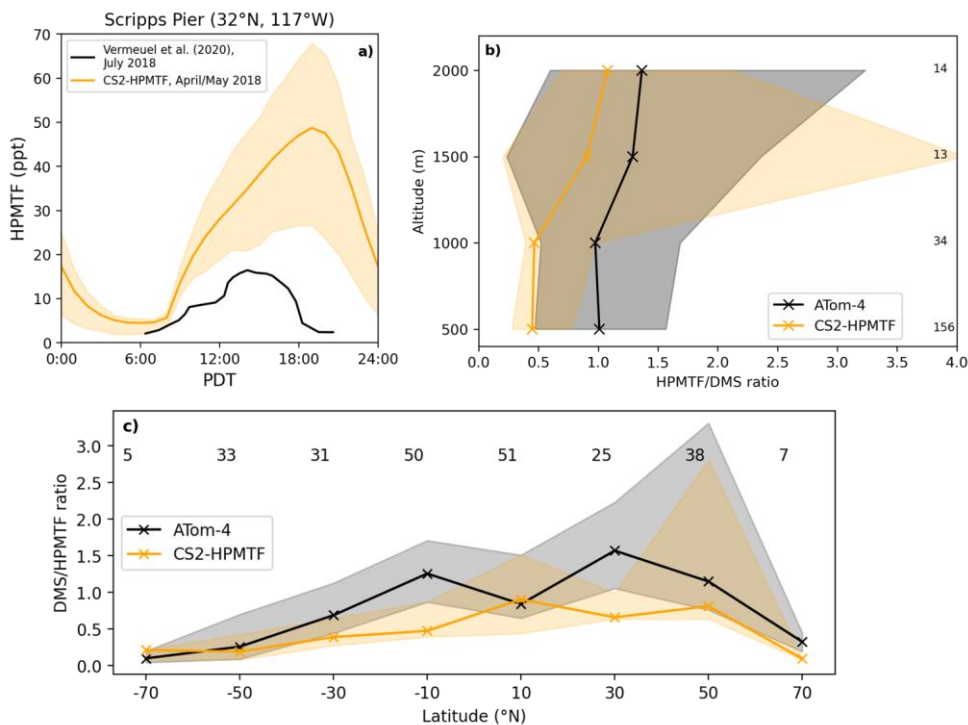
Figure 140: Seasonal average **a)** Global distribution of HPMTF mixing ratios in the lower troposphere (< 2 km) over the ocean in CS2-HPMTF. Annual means of the vertical distribution of HPMTF are shown in **b)** the Central North Atlantic (30-50°E, 20-45°N) and **c)** the Southern Ocean (50-70°S). The envelopes represent the interquartile range of the model data.

Comparison of HPMTF with observations

Since DMS in the model is likely overestimated, the same would be expected for HPMTF. **Figure 112a** shows that the implemented loss processes in CS2-HPMTF already lead to a diel profile of HPMTF that is similar to the one measured by

Development and intercomparison of DMS oxidation mechanisms

728 Vermeuel et al. (2020) (where no DMS measurements were made), without the need to add aqueous loss or photolysis. While
 729 DMS at low altitudes was overestimated by a factor of 5 in the model (see SI), the maximum HPMTF is only 3.7 times higher
 730 than the highest measurement in the diel profile at Scripps Pier (Figure 112a). For the comparison with ATom-4 data (Figure
 731 112b,c), the DMS/HPMTF is used to account for the discrepancy between DMS concentrations observed and in the model.
 732 The model generally underestimates the HPMTF/DMS ratio. For instance, up until 1000 m, the ratio in the model is half of
 733 the measured ratio. These results indicate that loss processes of HPMTF might still be too fast in the model or the oxidation of
 734 DMS too slow. The CS₂ oxidants have been evaluated before (Archer-Nicholls et al., 2021) and were found to be higher in
 735 the boundary layer than in ST simulations used in CMIP6 studies but well within the spread of other models (Griffiths et al.,
 736 2021; Stevenson et al., 2020).



738
 739 **Figure 121:** a) Comparison of the diel profile of HPMTF at the Scripps Pier at the California Coast (32°N, 117°W). The
 740 observational data (Vermeuel et al., 2020) is the mean of measurements from July 26 to August 3, 2018, while the model

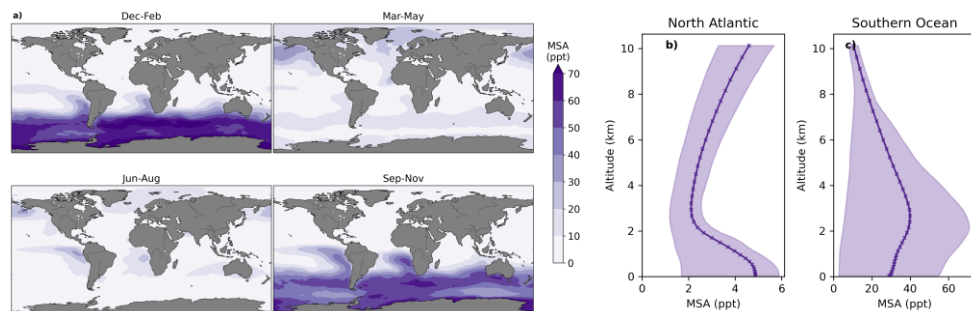
Development and intercomparison of DMS oxidation mechanisms

741 output is the mean from April/May 2018. **(b)** Vertically binned (500 m) and **(c)** latitudinally binned (20°) median
742 DMS/HPMTF ratio along the AToM-4 flight path. The envelopes represent the interquartile range of the measurements and
743 the respective model results while the numbers on the side/on top give the number of measurements in the respective bin.

745 4.2.2 Modelled MSA

746 MSA is an important intermediate of the OH-addition channel. It contributes to aerosol-growth and might play a role in new
747 particle formation (Chen et al., 2015; Chen and Finlayson-Pitts, 2017). MSA production is reduced from 7.9 Tg S yr⁻¹ in CS2
748 by 70% to 2.4 Tg S yr⁻¹ in CS2-HPMTF. In the CS2-HPMTF simulation, wet and dry deposition and gas-phase oxidation by
749 OH to CH₂SO₂ have been included as loss processes for MSA, which account for 89%, 10%, and 1% of the loss of MSA,
750 respectively. The tropospheric MSA burden is 40 Gg S in CS2-HPMTF with a lifetime of 6 days.

751
752 In CS2-HPMTF, MSA is greatest in the Southern Ocean (**Figure 13**), where it shows a strong seasonal pattern, similar to
753 DMS. Mixing ratios up to 80 ppt are reached in January (Austral summer), while in July they are below 10 ppt. This is reflected
754 in the big interquartile range of MSA in the Southern Ocean (**Figure 13c**). Since the OH addition pathway is negatively
755 temperature dependent, MSA is primarily produced at high latitudes, inversely to HPMTF. MSA shows the greatest asymmetry
756 in concentration between the North Atlantic and Southern Ocean out of the different species discussed here. As well as
757 significant differences between the magnitude of MSA simulated in the North Atlantic and Southern Ocean, the vertical
758 profiles of MSA are shown to be very different. MSA reaches a peak in concentration at around 2 km altitude in the Southern
759 Ocean (consistent with a longer DMS lifetime and therefore greater vertical transport), whereas it peaks near the surface in the
760 North Atlantic.



763 **Figure 13:** a) Global distribution of MSA mixing ratios in the lower troposphere (< 2 km) in CS2-HPMTF. Annual means of
764

Development and intercomparison of DMS oxidation mechanisms

the vertical distribution of MSA are shown in the **b)** Central North Atlantic (30-50°E, 20-45°N) and **c)** Southern Ocean (50-70°S). The envelopes represent the interquartile range of the measurements. Note the order of magnitude difference in the MSA concentrations in panels **b)** and **c)**.

4.2.23 Modelled SO₂ and sulfate

In CS2-HPMTF the SO₂ burden is increased by 5.6% compared with CS2, to 391 Gg S (**Table 4**). While this percentage seems low, a significant contribution to the SO₂ burden stems from anthropogenic sources and is mainly located above the land. The increase of SO₂ over the remote ocean, especially over the Southern Ocean, can reach up to 400% (**Figure 142**). At high latitudes, the new chemistry implemented in CS2-HPMTF also introduces a stronger seasonality to SO₂, whereby SO₂ concentration is higher in respective warmer months than in CS2 (**Figure 142, Figure S150a**). Comparison of CS2-HPMTF with ST reveals that the SO₂ burden is 9.2% higher in the ST run, which uses a 100% SO₂ yield from DMS (**Figure S78** in the SI). The global annual tropospheric sulfate burden is increased in CS2-HPMTF by 3.7% compared with CS2, to 604 Gg S. However, the sulfate burden is 5.3% higher in ST than in CS2-HPMTF (**Table 4**).

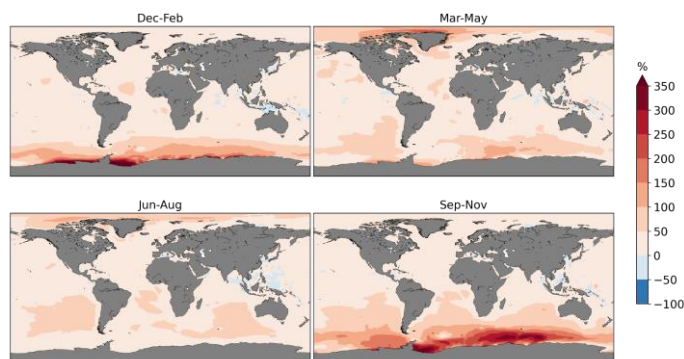
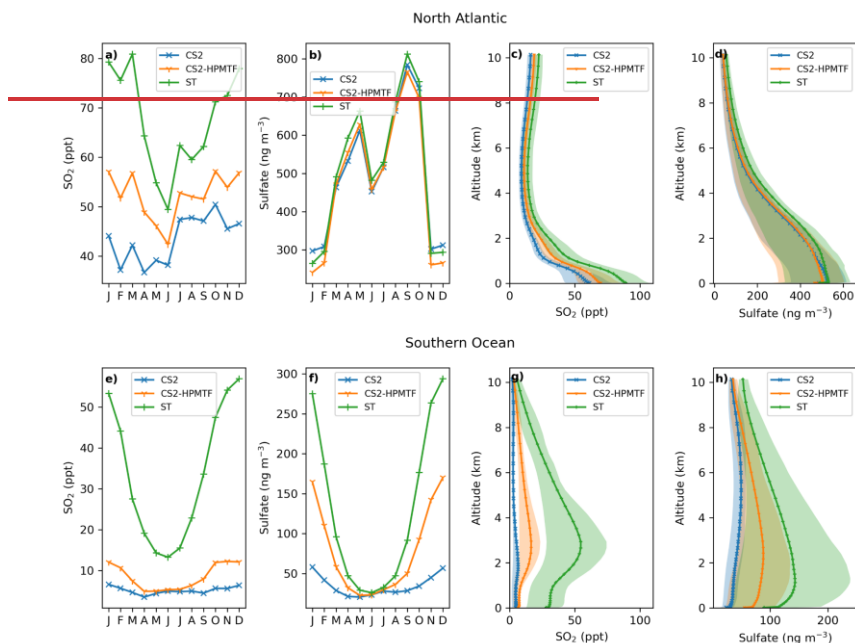


Figure 142: Relative difference in SO₂ mixing ratios in the lower troposphere (< 2 km) between CS2-HPMTF and the base run CS2 (CS2-HPMTF - CS2). Only values above the ocean are shown.

Comparing the three schemes, ST, CS2 and CS2-HPMTF, ST generally has the highest concentrations in SO₂ or sulfate and CS2 the lowest. The difference between the SO₂ mixing ratios in the different schemes is greatest in January/December and lowest in June, both in the Central North Atlantic and the Southern Ocean. This pattern is similar for sulfate concentrations in

Development and intercomparison of DMS oxidation mechanisms

the Southern Ocean, while sulfate in the North Atlantic is not affected by the different chemical schemes, resulting in similar concentrations for all simulations (due to the large contribution of anthropogenic sources). Additionally, here, sulfate concentration does not follow the same seasonal pattern as SO_2 , contrary to the Southern Ocean, where anthropogenic emissions are minimal. In the North Atlantic, the maximum SO_2 and sulfate levels are reached close to the surface (Figure 15c,d), tied closely to the fact that the major emissions—shipping and industry—are injected near the surface). SO_2 is depleted quickly in the boundary layer (similar to HPMTF in Figure 11), while sulfate concentrations decrease more slowly with height, owing to longer timescales for secondary production from intermediate lifetime DMS oxidation products. In the Southern Ocean however, the maximum SO_2 concentration is only reached at ~2 km in CS2 and ~3 km in CS2-HPMTF and ST. The opposite pattern is observed for the annual-mean maximum sulfate concentration by altitude: 1.1 km for ST, 2.4 km for CS-HPMTF and 5.2 km for CS2. This can affect the climate response to DMS emissions because radiative forcing is sensitive to the altitude of aerosols (Krishnamohan et al., 2019). Ranjithkumar et al. (2021) also assessed the ability of UKCA to simulate SO_2 compared with ATom measurements. In their study they used the Lana et al. (2011) emissions and found that reducing the scaling factor to that used by Mulcahy et al. (2018), amongst other changes (cloud pH and aerosol microphysical process changes) gave them the best fit to observations.



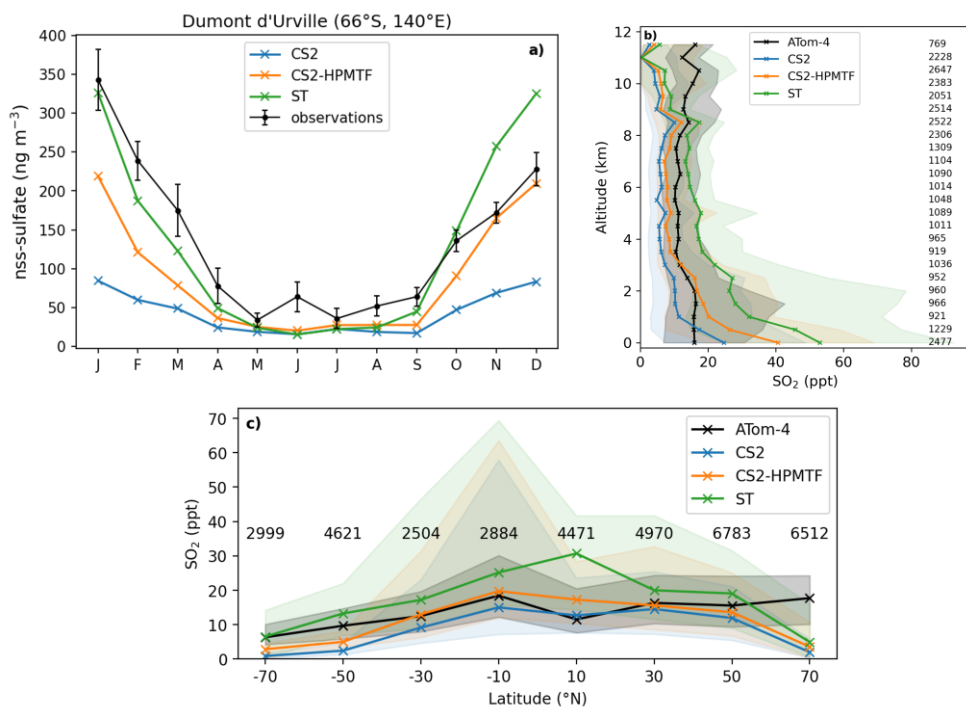
802 **Figure 15:** Monthly-mean (a) SO₂-mixing ratios (b) sulfate concentration in the lower troposphere (<2 km) and the annual
803 mean-vertical distribution of (c) SO₂ and (d) sulfate concentration in the Central North Atlantic (30–50°E, 20–45°N). The
804 envelopes represent the interquartile range of the measurements. (e)–(h) the equivalent for the Southern Ocean (50–70°S).
805

806 Comparison to observed SO₂ and sulfate

807 **Figure 136a** shows the monthly means of observed non-sea-salt sulfate (nss-sulfate) concentration at Dumont d'Urville station
808 (66°S, 140°E) between 1991 and 1995 (Minikin et al., 1998) and compares it to the sulfate concentration in the three different
809 UKCA model runs. The seasonal changes in sulfate concentrations are reproduced by CS2-HPMTF and ST, but not by CS2.
810 From April to September all three runs match the observations adequately well. Earlier in the year, the results from the ST run
811 match the observations best, while later in the year CS2-HPMTF reproduces the measurements better.
812

813 **Figure 136b,c** show SO₂ measurements along the ATom-4 flight path in comparison with the modelled SO₂ concentrations.
814 In the boundary layer, all runs over-predict SO₂ in comparison to the ATom-4 data (**Figure 136b**). In addition to wet and dry
815 deposition (Faloona 2009; Ranjithkumar et al., 2021), vertical mixing has been identified as a major source of uncertainty in
816 models (Gerbig et al., 2008) and could provide an explanation for the mismatch between the simulation results and
817 observations. At altitudes above 1.8 km, CS2-HPMTF is able to reflect SO₂ concentrations better than the other schemes.
818 Above 9 km, the simulations underestimate SO₂, potentially indicating issues with convective transport. Overall, in the ATom-
819 4 observations, SO₂ stays broadly constant with altitude, suggesting significant secondary sources or efficient vertical transport,
820 while in the simulations it decreases. Additionally, the interquartile ranges of the concentrations in each bin are bigger,
821 indicating a greater variance of model results than measured values. Overall, the mean SO₂ concentrations by the models in
822 each latitude bin predict the mean observation values well (**Figure 163c**). However, the variation of values is again greater in
823 the model, especially at low latitudes. The underestimation of SO₂ at 70°N could be due to an underestimation of the influence
824 of anthropogenic SO₂ emissions or unrealistic deposition of SO₂ (Hardacre et al., 2021). Alternatively, the SO₂ production
825 from DMS might be too slow still.
826
827

828



829

830 **Figure 163:** **a)** Comparison of nss-sulfate concentration at the Dumont d'Urville Station (66°S, 140°E) at the coast of
 831 Antarctica. The observational data stems from Minikin et al. (1998) and represents the monthly mean concentrations and their
 832 standard deviations for the years 1991-1995. **(b)** Vertically binned (500 m) and **(c)** latitudinally binned (20°) median SO_2
 833 mixing ratio along the ATom-4 flight path. The envelopes represent the interquartile range of the measurements and the
 834 respective model results while the numbers on the side/on top give the number of measurements in the respective bin.

835

836

837 4.3 Sensitivity runs

838 To improve our understanding of the variability of the model results, based on the uncertainties of HPMTF formation and loss,
 839 three sensitivity runs were conducted (CS2-HPMTF-CLD, CS2-HPMTF-FL, CS2-HPMTF-FP, **Table 1**). Loss of HPMTF to

Development and intercomparison of DMS oxidation mechanisms

840 clouds was proposed to be a major loss pathway by Veres et al. (2020) and Vermeuel et al. (2020). CS2-HPMTF-CLD adds
 841 cloud and aqueous uptake of HPMTF with a reactive uptake coefficient, γ , of 0.01, used in the study by Novak et al. (2021).
 842 Jernigan et al. (2022) recently established a rate constant for oxidation of HPMTF by OH as $1.4 (0.27\text{--}2.4) \times 10^{-11} \text{ cm}^3 \text{ molecule}^{-1}$
 843 s^{-1} through constrained chamber modelling using a rate constant for the formation of HPMTF as 0.1 s^{-1} . Ye et al. (2022) also
 844 measured the rate constant for this reaction. In their study they derived a rate constant of $2.1 \times 10^{-11} \text{ cm}^3 \text{ molecule}^{-1} \text{ s}^{-1}$ and an
 845 isomerization rate constant, k_{isom} , of $0.13 \pm 0.03 \text{ s}^{-1}$ at 295 K. Whilst, Further-further laboratory studies would be helpful in
 846 constraining this-the rate constant for OH + HPMTF, we recommend future work go into constraining the products of this
 847 reaction. Vermeuel et al. (2020) found the theoretically calculated rate constant $1.4 \times 10^{-12} \text{ cm}^3 \text{ molecule}^{-1} \text{ s}^{-1}$ by Wu et al. (2015)
 848 too slow and proposed a rate constant of $1.11 \times 10^{-11} \text{ cm}^3 \text{ molecule}^{-1} \text{ s}^{-1}$ instead, based on structurally similar molecules and
 849 modelling of their ground-based observations, similar to what we used in CS2-HPMTF. They recommend an upper limit of
 850 $5.1 \times 10^{-11} \text{ cm}^3 \text{ molecule}^{-1} \text{ s}^{-1}$ for the HPMTF+OH rate constant. Khan et al. (2021) and Novak et al. (2021) use $5.5 \times 10^{-11} \text{ cm}^3$
 851 $\text{molecule}^{-1} \text{ s}^{-1}$ for sensitivity tests, which was also employed in CS2-HPMTF-FL. Further, the study by Ye et al. (2021) looked
 852 at the uncertainty of the HPMTF isomerization rate. They estimate the isomerization rate constant as 0.09 s^{-1} ($0.03\text{--}0.3 \text{ s}^{-1}$, $1\sigma_{\text{g}}$
 853 geometric standard deviation at 293 K). Veres et al. (2020) are on the lower end of this range (0.041 s^{-1}) and Berndt et al.
 854 (2019) at the higher end (0.23 s^{-1}). The CS2-HPMTF-FP simulation scales the rate constant of Veres et al. (2020) by a factor
 855 of 5 to match Berndt's measurements at 295 K to examine the effects of higher HPMTF production. This rate constant was
 856 also used by Wollesen de Jonge et al. (2021) in their study. The annual mean of global tropospheric burdens of relevant species
 857 in these sensitivity runs are compared in **Table 4**.

858
 859 **Table 4:** Global annual mean tropospheric burdens of atmospheric sulfur species in UKCA base and sensitivity runs (first half
 860 of the table) and comparison to literature values (second half of the table, same acronyms as in Section 3)

Run	HPMTF burden (Gg S)	SO ₂ burden (Gg S)	Sulfate burden (Gg S)
CS2	-	370.1	582.3
ST	-	469.7	635.9
CS2-HPMTF	23.7	390.7	604.0
CS2-HPMTF-CLD	2.6	367.3	591.2
CS2-HPMTF-FL	8.9	392.6	605.6
CS2-HPMTF-FP	26.5	389.6	601.5
FG [⊗] (similar to CS2-HPMTF)	18	365	582
NV Base 1 [⊕] (similar to CS2-HPMTF)	18.8	189.0	526.7
NV Test 3 [⊕] (similar to CS2-HPMTF-CLD)	0.7	180.2	550.7
KH NEW_CHEM1 [⊗] (similar to CS2-HPMTF, with photolysis of HPMTF)	15.1	-	-
KH NEW_CHEM2 [⊗] (similar to CS2-HPMTF-FL)	6.1	-	-

Formatted: Font: Italic

Formatted: Font: Italic, Subscript

Formatted: Superscript

861 [Ⓢ]Fung et al., 2021; [Ⓠ]Novak et al., 2021; [Ⓞ]Khan et al., 2021.

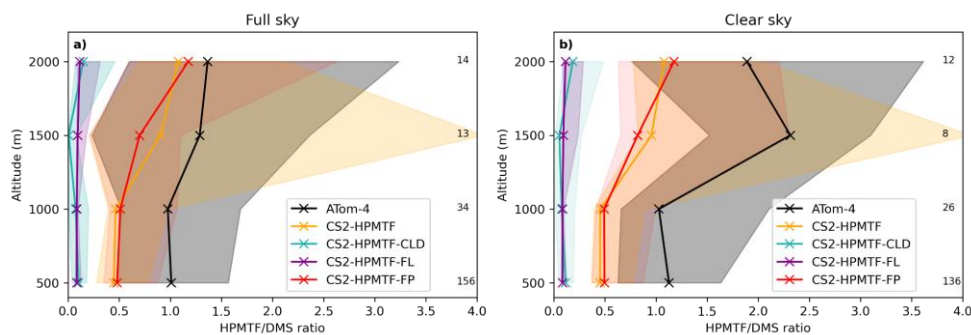
862 4.3.1 HPMTF

863 The HPMTF burden varies between 2.6 and 26.5 Gg S among the sensitivity runs (**Table 4**). Compared to CS2-HPMTF, faster
 864 OH oxidation reduces the HPMTF burden by -62% to 8.9 Gg S, while the addition of cloud and aqueous uptake to the scheme
 865 reduces it by -91% to only 2.6 Gg S. Yet, a factor of 5 higher production rate constant of HPMTF only leads to a 12% increase
 866 of HPMTF burden to 26.5 Gg S; suggesting that the steady-state distribution of HPMTF is controlled by the loss rate, not the
 867 rate of production of HPMTF. With the isomerization rate constant recommended by Veres et al. (2020), 51% of DMS forms
 868 HPMTF (86% of MTMP); with the faster rate in CS2-HPMTF-FP it is 57% (96% of MTMP). Since the use of the isomerization
 869 rate from Veres et al. (2020) already outcompetes the bimolecular reactions of MTMP, scaling the A-factor does not have a
 870 significant effect on the HPMTF yield from DMS. Overall, it can be estimated that globally 50-60% of DMS forms HPMTF
 871 (however, if more DMS is oxidised through the addition channel by BrO or multiphase reactions, this ratio could be lower).
 872 Consequently, HPMTF formation seems to be well constrained and the major uncertainties lie with the loss of HPMTF, which
 873 warrant additional measurements.

874

875 Similar to **Figure 112**, the HPMTF:DMS ratio is used in **Figure 174** to compare the results of the sensitivity model runs with
 876 ATom-4 observations. In general, schemes with a higher production and slower loss of HPMTF match the observations better,
 877 however, they still underestimate the measured ratios. A comparison was made to HPMTF:DMS ratios measured with no
 878 clouds present. Under these clear-sky conditions, when cloud uptake of HPMTF should not play a role in the measurements,
 879 observed ratios were even higher, leading to a greater difference between model results (which include clouds) and
 880 observations.

881



882

Development and intercomparison of DMS oxidation mechanisms

883 **Figure 174:** Vertically binned (500 m) median HPMTF/DMS ratio along the ATom-4 flight path for **a)** full sky and **b)** clear
884 sky, where measurements made in clouds are omitted. The envelopes represent the interquartile range of the measurements
885 and the respective model results, while values on the side give the number of measurements in the respective bin. Note that
886 the model data is the same in both panels.
887
888

889 4.3.2 SO₂

890 The SO₂ burden varies between 367.3 Gg S in CS2-HPMTF-CLD and 392.6 GgS in CS2-HPMTF-FL, suggesting that the SO₂
891 burden is relatively unaffected by the chemical sensitivities explored when compared with the much larger SO₂ burden simulated
892 with ST (469.7 Gg S); mainly due to the 100% DMS-SO₂ yield (**Table 4**).

893
894 CS2-HPMTF, CS2-HPMTF-FL, and CS2-HPMTF-FP have a higher SO₂ burden than CS2 since the changes to the abstraction
895 pathway (reaction 6a, 7c) and the addition of the isomerization pathway lead to more direct SO₂ production. Faster OH
896 oxidation of HPMTF in CS2-HPMTF-FL reduces the amount of HPMTF deposited and therefore increases the SO₂ burden
897 slightly (by 0.5%) compared to CS2-HPMTF. The faster production of HPMTF in CS2-HPMTF-FP reduces SO₂ burden
898 marginally (-0.3%), due to more sulfur now being deposited as HPMTF or forming OCS. The addition of cloud and
899 heterogeneous loss in CS2-HPMTF-CLD leads to immediate sulfate production instead of SO₂ formation, reducing the SO₂
900 burden by -6% compared to CS2-HPMTF, resulting in the lowest SO₂ burden in all runs considered.

902 4.4.3 Sulfate

903 In the sensitivity runs, the sulfate burdens are all higher than in the CS2 run (582.3 Gg S) and lower than in the ST run (635.9
904 Gg S). The variation by approximately 15 Gg S, from 591.2 Gg S in CS2-HPMTF-CLD to 605.6 Gg S in CS2-HPMTF-FL, is
905 smaller than the variation in sulfate burden simulated by similar mechanistic sensitivity tests by Novak et al. (2021) (~24 Gg),
906 suggesting some structural dependence on the results of the sensitivity tests (e.g., resolution, other model parameters). The
907 sulfate burdens in CS2-HPMTF-FL and CS2-HPMTF-FP behave similarly to CS2-HPMTF. Since CS2-HPMTF-CLD added
908 direct sulfate formation, a higher sulfate burden was expected. However, this was not seen in the experiments. Inspection of
909 the sulfate aerosol distribution shows that CS2-HPMTF-CLD leads to an increase in the coarse mode sulfate and a concomitant
910 reduction in sulfate aerosol lifetime (through an increase in wet deposition).

913 **5 Discussion**

914 The results described above demonstrate the global scale changes in the distribution of DMS and its oxidation products, through
915 the incorporation of improved mechanistic updates into the UKCA model. Here we discuss our results in the context of the
916 existing literature.

917 **5.1 DMS**

918 The DMS burden of 63-66 Gg S in this work is in good agreement with recent modelling studies (50 Gg S in Fung et al. (2022),
919 74 Gg S in Chen et al. (2018)). However, as shown in [the supplement, Section-S24.1.1.1](#), the modelled DMS concentrations do
920 not match observational measurements. One explanation could be underestimation of DMS oxidation. Here, only oxidation by
921 OH and NO₃ is included. However, Fung et al. (2022), who include oxidation by BrO, O₃ and Cl (accounting in total for 20%
922 of DMS depletion), also found that their model over-predicted DMS mixing ratios compared to the ATom-4 measurements.
923 Inadequate representation of DMS concentrations in seawater and therefore emissions contribute to the largest uncertainties in
924 the sulfur budget (Tesdal et al., 2016; Bock et al., 2021) and could explain most of the difference. Additionally, physical
925 differences between model and observation, such as wind speed and temperature, and a poor space resolution of Whole Air
926 Sampling might also play a role. Crucially, more long-term observations of DMS in the atmosphere are needed to complement
927 works that have collated oceanic DMS observations (e.g., Lana et al., 2011).

928
929 Here, in all model runs 75% of DMS is oxidised by OH and 25% by NO₃. Other studies found global contributions of OH
930 between 50-70% and NO₃ 15-30% (Boucher et al., 2003; Berglen et al., 2004; Breider et al., 2010; Khan et al., 2016; Chen et
931 al., 2018; Fung et al., 2022). The lower contribution of OH oxidation to DMS removal is explained by the addition of other
932 pathways, such as oxidation by BrO, Cl and multiphase reactions. Consequently, the lifetime of 1.5 days for DMS in this work
933 is longer than some other studies including these reactions (e.g., 0.8 days in Fung et al. (2022) and 1.2 days in Chen et al.
934 (2018)). Nonetheless, it is well within the range of 0.9 to 5 days (with a mean of 2 days) of the models examined in Faloon
935 (2009).

938 **5.2 HPMTF**

939 In CS2-HPMTF 51% of DMS forms HPMTF. With a faster formation of HPMTF, found in laboratory experiments, this yield
940 increases to 57% in our model. The yield could possibly be lower if other oxidation reactions of DMS are included that follow
941 the OH addition pathway (multiphase reactions, oxidation by BrO), [which was omitted in this work](#). Veres et al. (2020),
942 [Novak et al. \(2021\) and Fung et al. \(2022\)](#) estimated that at least 30-46% of DMS was forming HPMTF, based on [their](#)
943 observationally constrained modelling of *in situ* or laboratory data. Even though the rate of HPMTF formation is uncertain

Formatted: Font: Italic

Development and intercomparison of DMS oxidation mechanisms

(Ye et al., 2021), it does not significantly affect the HPMTF yield from DMS, since it already outcompetes most other reactions of MTMP. For HPMTF formation, uncertainty seems to lie mainly at the branching ratio of the addition and the abstraction pathway of DMS. Indeed, the uncertainty in the HPMTF burden stems from the uncertainty ~~of~~ in the loss pathways and their respective contribution to HPMTF loss. Our model results agree well with the HPMTF burdens obtained by other global modelling studies, both in absolute values but also the relative changes we find in the sensitivity study (**Table 4**) (e.g., Fung et al. (2022)): In our sensitivity study a faster oxidation of HPMTF to OH lead to a decrease of 62% of the HPMTF burden, in Khan et al. (2021) it was 60%. In this work the addition of aqueous uptake of HPMTF reduced the burden by 91%, very similar to the reduction simulated in Novak et al. (2021) (96%).

5.3 MSA

The tropospheric MSA burden is 40 Gg S in CS2-HPMTF with a lifetime of 6 days. This falls within the range of 13-40 Gg S and a lifetime of 5-7 days found in previous model studies (Pham et al., 1995; Chin et al., 1996, 2000; Cosme et al., 2002; Hezel et al., 2011). However, newer studies include more multiphase processes and usually tend to have shorter lifetimes and lower MSA burdens. Both the scheme in Fung et al. (2022) and Chen et al. (2018), include the loss of MSA to aqueous OH oxidation, resulting in lifetimes of 0.6 days and 2.2 days and a burden of 8 Gg S and 20 Gg S, respectively.

5.4 SO₂ and Sulfate

Comparing SO₂ and sulfate burdens with other modelling studies is more challenging, since those species can have other sources apart from DMS. That said, our SO₂ obtained in the various runs based on the CS2 scheme are comparable to Fung et al. (2022), while the ST burden is significantly higher. However, the SO₂ burden from Novak et al. (2021) is much lower. This difference cannot be explained solely by differences in the DMS oxidation mechanism; more likely, the difference is in anthropogenic SO₂ emissions.

The sulfate burden in all our runs fall within the range found in other recent modelling studies (Chen et al. 2018; Novak et al., 2021; Fung et al., 2022). Considering the relative change due to the addition of the isomerization pathway, the increase in sulfate burden from CS2 to CS2-HPMTF is only 3.7% in our study, Fung et al. (2022) found an increase of 8.8%, when they added HPMTF chemistry. However, unlike their results, we find strong seasonality in the additional sulfate produced, especially in the Southern Hemisphere. The addition of cloud uptake and direct sulfate formation in CS2-HPMTF-CLD decreased the sulfate burden in our study by (-)2.2%, in Novak et al. (2021) this change in mechanism lead to an increase of sulfate by 4.5%.

5.5 Comparison with BOXMOX results.

In Section 3 and Section 4 we have shown the results of BOXMOX and UKCA simulations using different DMS mechanistic variants respectively. Whilst the same mechanistic variants have been assessed in both model setups, it is not possible to

Development and intercomparison of DMS oxidation mechanisms

976 directly compare the results of the two sets of experiments because of the large differences in the model setups used. However,
977 some qualitative comparisons can be made. For MSA, Section 3.1 (Figure 2) suggests that the MSA simulated with CS2-
978 HPMTF should be much lower than CS2; as is calculated in Section 4.2.2 (a 70% reduction). For SO₂, both the BOXMOX
979 and UKCA results agree in the ordering of simulations, ST, CS2 and CS2-HPMTF; with ST simulating significantly more SO₂
980 than the other mechanisms. However, whereas BOXMOX simulations suggest that H₂SO₄ is predicted to be higher in CS2 and
981 CS2-HPMTF than ST, the UKCA model runs suggest that ST has the greatest burden of sulfate; highlighting the complexity
982 of making inference on aerosols from gas phase precursors in box model studies.
983

984 **6 Conclusion**

985 DMS remains an important molecule in our understanding of the background aerosol budget and the uncertainty of aerosols
986 to climate change (Carslaw et al., 2013). In this study we have used a combination of box modelling experiments and global
987 3D model experiments to explore the sensitivities of the DMS oxidation mechanism in the UKCA model. This work has
988 delivered a new DMS oxidation mechanism for use within the CRI-Strat framework of UKCA (Archer-Nicholls et al., 2021;
989 Weber et al., 2021), which is a significant advancement and improvement over the mechanism used in CMIP6 studies
990 (Archibald et al., 2020). Our new DMS mechanism includes many of the recently discovered and proposed oxidation pathways
991 for DMS and through the series of experiments we have performed, we have been able to benchmark this scheme against other
992 recently reported schemes in the literature. Whilst future studies building on the ever expanding database of laboratory studies
993 (e.g., Ye et al., 2021; Jernigan et al., 2022) are required to refine the DMS oxidation mechanism further, with the current
994 availability of observational data, it is not possible to fully constrain the uncertain parameters in the DMS oxidation
995 mechanism. Hence there is a priority for more observational based studies that combine ship, ground-based and aircraft
996 platforms optimally. Fung et al. (2021) have shown that there are consequences for radiative forcing by updating the DMS
997 mechanism in the CESM model, and follow up work will investigate these changes with UKCA.
998

999 This study adds to the few other mechanism intercomparisons that exist in the literature, spanning back more than 25 years
1000 (Capaldo and Pandis 1997; Karl et al., 2007). Similar to these other studies we find that MSA is particularly uncertain when it
1001 comes to the results obtained using the range of mechanisms that we investigated. Further work should explicitly focus on
1002 reducing uncertainty in the MSA budget in the atmosphere, especially given its potential importance in reconstructing paleo-
1003 sea ice (Thomas et al., 2019).
1004

1005 In many ways, the recent advances in DMS oxidation chemistry are similar to isoprene chemistry, where over a decade ago
1006 the discovery of uni-molecular isomerisation reactions resulted in a step-change in our understanding of isoprene. As with
1007 isoprene, ever more complex and faithful descriptions of DMS chemistry will be delivered over the coming years. But the

Development and intercomparison of DMS oxidation mechanisms

1008 biggest challenge (as for isoprene) will remain in reducing and accurately distilling down this complex chemistry for use in
1009 global model studies, and in characterising the sources of DMS into the atmosphere (which for isoprene have only recently
1010 been possibly directly e.g., Wells et al., 2020).

1011

1012 **Acknowledgements**

1013 BAC thanks the Studienstiftung des Deutschen Volkes for financial support. We would like to thank NERC through the ACSIS
1014 (NE/N018001/1) and CARES projects for funding (NE/W009412/1). We would like to thank the UK Met Office JWCRP and
1015 Clean Air programmes and the National Centre for Atmospheric Science for funding the development of the UKCA model.
1016 LER acknowledges support from the Deep South National Science Challenge (contract C01X1901). ATA thanks the
1017 University of Canterbury Erskine Programme. This work used Monsoon2, a collaborative high-performance computing facility
1018 funded by the Met Office and the Natural Environment Research Council. This work used JASMIN, the UK collaborative data
1019 analysis facility.

1020

1021 **Competing interests**

1022 The authors declare no competing interests.

Development and intercomparison of DMS oxidation mechanisms

1023 **References**

1024 [Assaf, E., Finewax, Z., Marshall, P., Veres, P.R., Neuman, J.A. and Burkholder, J.B.: Measurement of the Intramolecular](#)
1025 [Hydrogen-Shift Rate Coefficient for the CH₃SCH₂OO Radical between 314 and 433 K. *The Journal of Physical Chemistry*](#)
1026 [A, 127\(10\), pp.2336-2350, 2023.](#)

1027 Andreae, M. O.: Ocean-atmosphere interactions in the global biogeochemical sulfur cycle, *Marine Chemistry*, 30, 1–29,
1028 [https://doi.org/10.1016/0304-4203\(90\)90059-L](https://doi.org/10.1016/0304-4203(90)90059-L), 1990.

1029 Archer-Nicholls, S., Abraham, N. L., Shin, Y. M., Weber, J., Russo, M. R., Lowe, D., Utembe, S. R., O'Connor, F. M.,
1030 Kerridge, B., Latter, B., Siddans, R., Jenkin, M., Wild, O., and Archibald, A. T.: The Common Representative Intermediates
1031 Mechanism Version 2 in the United Kingdom Chemistry and Aerosols Model, 13, e2020MS002420,
1032 <https://doi.org/10.1029/2020MS002420>, 2021.

1033 Archibald, A. T., Jenkin, M. E., and Shallcross, D. E.: An isoprene mechanism intercomparison, *Atmospheric Environment*,
1034 44, 5356–5364, <https://doi.org/10.1016/j.atmosenv.2009.09.016>, 2010.

1035 Archibald, A. T., O'Connor, F. M., Abraham, N. L., Archer-Nicholls, S., Chipperfield, M. P., Dalvi, M., Folberth, G. A.,
1036 Dennison, F., Dhomse, S. S., Griffiths, P. T., Hardacre, C., Hewitt, A. J., Hill, R. S., Johnson, C. E., Keeble, J., Köhler, M. O.,
1037 Morgenstern, O., Mulcahy, J. P., Ordóñez, C., Pope, R. J., Rumbold, S. T., Russo, M. R., Savage, N. H., Sellar, A., Stringer,
1038 M., Turnock, S. T., Wild, O., and Zeng, G.: Description and evaluation of the UKCA stratosphere–troposphere chemistry
1039 scheme (StratTrop v1.0) implemented in UKESM1, 13, 1223–1266, <https://doi.org/10.5194/gmd-13-1223-2020>, 2020.

1040 Arsene, C., Barnes, I., and Becker, K. H.: FT-IR product study of the photo-oxidation of dimethyl sulfide: Temperature and
1041 O₂ partial pressure dependence, *Phys. Chem. Chem. Phys.*, 1, 5463–5470, <https://doi.org/10.1039/A907211J>, 1999.

1042 Atkinson, R., Baulch, D. L., Cox, R. A., Crowley, J. N., Hampson, R. F., Hynes, R. G., Jenkin, M. E., Rossi, M. J., and Troe,
1043 J.: Evaluated kinetic and photochemical data for atmospheric chemistry: Volume I - gas phase reactions of O_x, HO_x, NO_x and
1044 SO_x species, 4, 1461–1738, <https://doi.org/10.5194/acp-4-1461-2004>, 2004.

1045 Barnes, I., Hjorth, J., and Mihalopoulos, N.: Dimethyl Sulfide and Dimethyl Sulfoxide and Their Oxidation in the Atmosphere,
1046 *Chem. Rev.*, 106, 940–975, <https://doi.org/10.1021/cr020529+>, 2006.

1047 Barone, S., A. Turnipseed, A., and R. Ravishankara, A.: Role of adducts in the atmospheric oxidation of dimethyl sulfide, 100,
1048 39–54, <https://doi.org/10.1039/FD9950000039>, 1995.

1049 Berglen, T. F., Bernsten, T. K., Isaksen, I. S. A., and Sundet, J. K.: A global model of the coupled sulfur/oxidant chemistry in
1050 the troposphere: The sulfur cycle, 109, <https://doi.org/10.1029/2003JD003948>, 2004.

Development and intercomparison of DMS oxidation mechanisms

1051 Berndt, T., Scholz, W., Mentler, B., Fischer, L., Hoffmann, E. H., Tilgner, A., Hyttinen, N., Prisle, N. L., Hansel, A., and
1052 Herrmann, H.: Fast Peroxy Radical Isomerization and OH Recycling in the Reaction of OH Radicals with Dimethyl Sulfide,
1053 *J. Phys. Chem. Lett.*, 10, 6478–6483, <https://doi.org/10.1021/acs.jpcllett.9b02567>, 2019.

1054 [Bhatti, Y., Revell, L., Schuddeboom, A., McDonald, A., Archibald, A., Williams, J., Venugopal, A., Hardacre, C., and](#)
1055 [Behrens, E.: The sensitivity of Southern Ocean atmospheric dimethyl sulfide to modelled sources and emissions, *EGUsphere*](#)
1056 [\[preprint\], <https://doi.org/10.5194/egusphere-2023-868>, 2023.](#)

1057 Bock, J., Michou, M., Nabat, P., Abe, M., Mulcahy, J. P., Oliví, D. J. L., Schwinger, J., Suntharalingam, P., Tjiputra, J., van
1058 Hulten, M., Watanabe, M., Yool, A., and Séférian, R.: Evaluation of ocean dimethylsulfide concentration and emission in
1059 CMIP6 models, 18, 3823–3860, <https://doi.org/10.5194/bg-18-3823-2021>, 2021.

1060 Borissenko, D., Kukui, A., Laverdet, G., and Le Bras, G.: Experimental Study of SO₂ Formation in the Reactions of CH₃SO
1061 Radical with NO₂ and O₃ in Relation with the Atmospheric Oxidation Mechanism of Dimethyl Sulfide, *J. Phys. Chem. A*,
1062 107, 1155–1161, <https://doi.org/10.1021/jp021701g>, 2003.

1063 Boucher, O., Moulin, C., Belviso, S., Aumont, O., Bopp, L., Cosme, E., von Kuhlmann, R., Lawrence, M. G., Pham, M.,
1064 Reddy, M. S., Sciare, J., and Venkataraman, C.: DMS atmospheric concentrations and sulphate aerosol indirect radiative
1065 forcing: a sensitivity study to the DMS source representation and oxidation, 3, 49–65, <https://doi.org/10.5194/acp-3-49-2003>,
1066 2003.

1067 Breider, T. J., Chipperfield, M. P., Richards, N. a. D., Carslaw, K. S., Mann, G. W., and Spracklen, D. V.: Impact of BrO on
1068 dimethylsulfide in the remote marine boundary layer, 37, <https://doi.org/10.1029/2009GL040868>, 2010.

1069 de Bruyn, W. J., Harvey, M., Caine, J. M., and Saltzman, E. S.: DMS and SO₂ at Baring Head, New Zealand: Implications
1070 for the Yield of SO₂ from DMS, *Journal of Atmospheric Chemistry*, 41, 189–209, <https://doi.org/10.1023/A:1014252106572>,
1071 2002.

1072 Butkovskaya, N. I. and Barnes, I.: Model Study of the Photooxidation of CH₃SO₂SCH₃ at Atmospheric Pressure: Thermal
1073 Decomposition of the CH₃SO₂ Radical, in: *Global Atmospheric Change and its Impact on Regional Air Quality*, edited by:
1074 Barnes, I., Springer Netherlands, Dordrecht, 147–152, https://doi.org/10.1007/978-94-010-0082-6_22, 2002.

1075 Butkovskaya, N. I. and LeBras, G.: Mechanism of the NO₃ + DMS Reaction by Discharge Flow Mass Spectrometry, *J. Phys.*
1076 *Chem.*, 98, 2582–2591, <https://doi.org/10.1021/j100061a014>, 1994.

1077 Caldeira, K. and Duffy, P.B. The role of the Southern Ocean in uptake and storage of anthropogenic carbon dioxide. *Science*,
1078 287(5453), pp.620-622. 2000.

Development and intercomparison of DMS oxidation mechanisms

- 1079 Campolongo, F., Saltelli, A., Jensen, N. R., Wilson, J., and Hjorth, J.: The Role of Multiphase Chemistry in the Oxidation of
1080 Dimethylsulphide (DMS). A Latitude Dependent Analysis, *Journal of Atmospheric Chemistry*, 32, 327–356,
1081 <https://doi.org/10.1023/A:1006154618511>, 1999.
- 1082 Cao, J., Wang, W.L., Gao, L.J. and Fu, F.: Mechanism and thermodynamic properties of CH_3SO_3 decomposition. *Acta*
1083 *Physico-Chimica Sinica*, 29(6), 1161-1167, <https://doi.org/10.3866/PKU.WHXB201304021>, 2013.
- 1084 Capaldo, K.P. and Pandis, S.N. Dimethylsulfide chemistry in the remote marine atmosphere: Evaluation and sensitivity
1085 analysis of available mechanisms. *Journal of Geophysical Research: Atmospheres*, 102(D19), pp.23251-23267. 1997
- 1086
- 1087 Carslaw, K. S., Lee, L. A., Reddington, C. L., Pringle, K. J., Rap, A., Forster, P. M., Mann, G. W., Spracklen, D. V.,
1088 Woodhouse, M. T., Regayre, L. A., and Pierce, J. R.: Large contribution of natural aerosols to uncertainty in indirect forcing,
1089 503, 67–71, <https://doi.org/10.1038/nature12674>, 2013.
- 1090 Charlson, R. J., Lovelock, J. E., Andreae, M. O., and Warren, S. G.: Oceanic phytoplankton, atmospheric sulphur, cloud albedo
1091 and climate, 326, 655–661, <https://doi.org/10.1038/326655a0>, 1987.
- 1092 Chen, H. and Finlayson-Pitts, B. J.: New Particle Formation from Methanesulfonic Acid and Amines/Ammonia as a Function
1093 of Temperature, *Environ. Sci. Technol.*, 51, 243–252, <https://doi.org/10.1021/acs.est.6b04173>, 2017.
- 1094 Chen, H., Ezell, M. J., Arquero, K. D., Varner, M. E., Dawson, M. L., Gerber, R. B., and Finlayson-Pitts, B. J.: New particle
1095 formation and growth from methanesulfonic acid, trimethylamine and water, *Phys. Chem. Chem. Phys.*, 17, 13699–13709,
1096 <https://doi.org/10.1039/C5CP00838G>, 2015.
- 1097 Chen, J., Berndt, T., Møller, K. H., Lane, J. R., and Kjaergaard, H. G.: Atmospheric Fate of the CH_3SOO Radical from the
1098 $\text{CH}_3\text{S} + \text{O}_2$ Equilibrium, *J. Phys. Chem. A*, 125, 8933–8941, <https://doi.org/10.1021/acs.jpca.1c06900>, 2021.
- 1099 Chen, Q., Sherwen, T., Evans, M., and Alexander, B.: DMS oxidation and sulfur aerosol formation in the marine troposphere:
1100 a focus on reactive halogen and multiphase chemistry, 18, 13617–13637, <https://doi.org/10.5194/acp-18-13617-2018>, 2018.
- 1101 Chin, M., Jacob, D. J., Gardner, G. M., Foreman-Fowler, M. S., Spiro, P. A., and Savoie, D. L.: A global three-dimensional
1102 model of tropospheric sulfate, 101, 18667–18690, <https://doi.org/10.1029/96JD01221>, 1996.
- 1103 Chin, M., Savoie, D. L., Huebert, B. J., Bandy, A. R., Thornton, D. C., Bates, T. S., Quinn, P. K., Saltzman, E. S., and Bruyn,
1104 W. J. D.: Atmospheric sulfur cycle simulated in the global model GOCART: Comparison with field observations and regional
1105 budgets, 105, 24689–24712, <https://doi.org/10.1029/2000JD900385>, 2000.

Development and intercomparison of DMS oxidation mechanisms

- 1106 Collins, W. J., Lamarque, J.-F., Schulz, M., Boucher, O., Eyring, V., Hegglin, M. I., Maycock, A., Myhre, G., Prather, M.,
1107 Shindell, D., and Smith, S. J.: AerChemMIP: quantifying the effects of chemistry and aerosols in CMIP6, 10, 585–607,
1108 <https://doi.org/10.5194/gmd-10-585-2017>, 2017.
- 1109 Cosme, E., Genthon, C., Martinerie, P., Boucher, O., and Pham, M.: The sulfur cycle at high-southern latitudes in the LMD-
1110 ZT General Circulation Model, 107, ACH 7-1-ACH 7-19, <https://doi.org/10.1029/2002JD002149>, 2002.
- 1111 Dee, D. P., Uppala, S. M., Simmons, A. J., Berrisford, P., Poli, P., Kobayashi, S., Andrae, U., Balmaseda, M. A., Balsamo, G.,
1112 Bauer, P., Bechtold, P., Beljaars, A. C. M., van de Berg, L., Bidlot, J., Bormann, N., Delsol, C., Dragani, R., Fuentes, M.,
1113 Geer, A. J., Haimberger, L., Healy, S. B., Hersbach, H., Hólm, E. V., Isaksen, I., Kållberg, P., Köhler, M., Matricardi, M.,
1114 McNally, A. P., Monge-Sanz, B. M., Morcrette, J.-J., Park, B.-K., Peubey, C., de Rosnay, P., Tavolato, C., Thépaut, J.-N., and
1115 Vitart, F.: The ERA-Interim reanalysis: configuration and performance of the data assimilation system, 137, 553–597,
1116 <https://doi.org/10.1002/qj.828>, 2011.
- 1117 Faloon, I.: Sulfur processing in the marine atmospheric boundary layer: A review and critical assessment of modeling
1118 uncertainties, *Atmospheric Environment*, 43, 2841–2854, <https://doi.org/10.1016/j.atmosenv.2009.02.043>, 2009.
- 1119 Fung, K. M., Heald, C. L., Kroll, J. H., Wang, S., Jo, D. S., Gettelman, A., Lu, Z., Liu, X., Zaveri, R. A., Apel, E., Blake, D.
1120 R., Jimenez, J.-L., Campuzano-Jost, P., Veres, P., Bates, T. S., Shilling, J. E., and Zawadowicz, M.: Exploring DMS oxidation
1121 and implications for global aerosol radiative forcing, 1–58, <https://doi.org/10.5194/acp-2021-782>, 2021.
- 1122 Galí, M., Lévassieur, M., Devred, E., Simó, R., and Babin, M.: Sea-surface dimethylsulfide (DMS) concentration from satellite
1123 data at global and regional scales, *Biogeosciences*, 15, 3497–3519, <https://doi.org/10.5194/bg-15-3497-2018>, 2018.
- 1124 Glasow, R. von, Sander, R., Bott, A., and Crutzen, P. J.: Modeling halogen chemistry in the marine boundary layer 1. Cloud-
1125 free MBL, 107, ACH 9-1-ACH 9-16, <https://doi.org/10.1029/2001JD000942>, 2002.
- 1126 Griffiths, P. T., Murray, L. T., Zeng, G., Shin, Y. M., Abraham, N. L., Archibald, A. T., Deushi, M., Emmons, L. K., Galbally,
1127 I. E., Hassler, B., Horowitz, L. W., Keeble, J., Liu, J., Moeini, O., Naik, V., O'Connor, F. M., Oshima, N., Tarasick, D., Tilmes,
1128 S., Turnock, S. T., Wild, O., Young, P. J., and Zanis, P.: Tropospheric ozone in CMIP6 simulations, *Atmos. Chem. Phys.*, 21,
1129 4187–4218, <https://doi.org/10.5194/acp-21-4187-2021>, 2021.
- 1130 Guenther, A. B., Jiang, X., Heald, C. L., Sakulyanontvittaya, T., Duhl, T., Emmons, L. K., and Wang, X.: The Model of
1131 Emissions of Gases and Aerosols from Nature version 2.1 (MEGAN2.1): an extended and updated framework for modeling
1132 biogenic emissions, 5, 1471–1492, <https://doi.org/10.5194/gmd-5-1471-2012>, 2012.
- 1133 Hezel, P. J., Alexander, B., Bitz, C. M., Steig, E. J., Holmes, C. D., Yang, X., and Sciare, J.: Modeled methanesulfonic acid
1134 (MSA) deposition in Antarctica and its relationship to sea ice, 116, <https://doi.org/10.1029/2011JD016383>, 2011.

Development and intercomparison of DMS oxidation mechanisms

- 1135 Ho, S., Peng, L., Anthes, R. A., Kuo, Y.-H., and Lin, H.-C.: Marine Boundary Layer Heights and Their Longitudinal, Diurnal,
1136 and Interseasonal Variability in the Southeastern Pacific Using COSMIC, CALIOP, and Radiosonde Data, *J. Climate*, 28,
1137 2856–2872, <https://doi.org/10.1175/JCLI-D-14-00238.1>, 2015.
- 1138 Hoesly, R. M., Smith, S. J., Feng, L., Klimont, Z., Janssens-Maenhout, G., Pitkanen, T., Seibert, J. J., Vu, L., Andres, R. J.,
1139 Bolt, R. M., Bond, T. C., Dawidowski, L., Kholod, N., Kurokawa, J., Li, M., Liu, L., Lu, Z., Moura, M. C. P., O'Rourke, P.
1140 R., and Zhang, Q.: Historical (1750–2014) anthropogenic emissions of reactive gases and aerosols from the Community
1141 Emissions Data System (CEDS), 11, 369–408, <https://doi.org/10.5194/gmd-11-369-2018>, 2018.
- 1142 Hoffmann, E. H., Tilgner, A., Schrödner, R., Brüer, P., Wolke, R., and Herrmann, H.: An advanced modeling study on the
1143 impacts and atmospheric implications of multiphase dimethyl sulfide chemistry, *PNAS*, 113, 11776–11781,
1144 <https://doi.org/10.1073/pnas.1606320113>, 2016.
- 1145 Hoffmann, E. H., Heinold, B., Kubin, A., Tegen, I., and Herrmann, H.: The Importance of the Representation of DMS
1146 Oxidation in Global Chemistry–Climate Simulations, 48, e2021GL094068, <https://doi.org/10.1029/2021GL094068>, 2021.
- 1147 Hulswar, S., Simó, R., Galí, M., Bell, T. G., Lana, A., Inamdar, S., Halloran, P. R., Manville, G., and Mahajan, A. S.: Third
1148 revision of the global surface seawater dimethyl sulfide climatology (DMS-Rev3), *Earth Syst. Sci. Data*, 14, 2963–2987,
1149 <https://doi.org/10.5194/essd-14-2963-2022>, 2022.
- 1150 Jenkin, M. E., Young, J. C., and Rickard, A. R.: The MCM v3.3.1 degradation scheme for isoprene, 15, 11433–11459,
1151 <https://doi.org/10.5194/acp-15-11433-2015>, 2015.
- 1152 Jenkin, M. E., Khan, M. A. H., Shallcross, D. E., Bergström, R., Simpson, D., Murphy, K. L. C., and Rickard, A. R.: The CRI
1153 v2.2 reduced degradation scheme for isoprene, *Atmospheric Environment*, 212, 172–182,
1154 <https://doi.org/10.1016/j.atmosenv.2019.05.055>, 2019.
- 1155 Jernigan, C.M., Fite, C.H., Vereecken, L., Berkelhammer, M.B., Rollins, A.W., Rickly, P.S., Novelli, A., Taraborrelli, D.,
1156 Holmes, C.D. and Bertram, T.H. Efficient Production of Carbonyl Sulfide in the Low-NOx Oxidation of Dimethyl Sulfide.
1157 *Geophysical Research Letters*, 49(3), p.e2021GL096838. 2022.
- 1158 Karl, M., Gross, A., Leck, C., and Pirjola, L.: Intercomparison of dimethylsulfide oxidation mechanisms for the marine
1159 boundary layer: Gaseous and particulate sulfur constituents, 112, <https://doi.org/10.1029/2006JD007914>, 2007.
- 1160 Khan, M. A. H., Gillespie, S. M. P., Razis, B., Xiao, P., Davies-Coleman, M. T., Percival, C. J., Derwent, R. G., Dyke, J. M.,
1161 Ghosh, M. V., Lee, E. P. F., and Shallcross, D. E.: A modelling study of the atmospheric chemistry of DMS using the global
1162 model, STOCHEM-CRI, *Atmospheric Environment*, 127, 69–79, <https://doi.org/10.1016/j.atmosenv.2015.12.028>, 2016.

Development and intercomparison of DMS oxidation mechanisms

- 1163 Khan, M. A. H., Bannan, T. J., Holland, R., Shallcross, D. E., Archibald, A. T., Matthews, E., Back, A., Allan, J., Coe, H.,
1164 Artaxo, P., and Percival, C. J.: Impacts of Hydroperoxymethyl Thioformate on the Global Marine Sulfur Budget, *ACS Earth*
1165 *Space Chem.*, 5, 2577–2586, <https://doi.org/10.1021/acsearthspacechem.1c00218>, 2021.
- 1166 Knote, C., Tuccella, P., Curci, G., Emmons, L., Orlando, J. J., Madronich, S., Baró, R., Jiménez-Guerrero, P., Luecken, D.,
1167 Hogrefe, C., Forkel, R., Werhahn, J., Hirtl, M., Pérez, J. L., San José, R., Giordano, L., Brunner, D., Yahya, K., and Zhang,
1168 Y.: Influence of the choice of gas-phase mechanism on predictions of key gaseous pollutants during the AQMEII phase-2
1169 intercomparison, *Atmospheric Environment*, 115, 553–568, <https://doi.org/10.1016/j.atmosenv.2014.11.066>, 2015.
- 1170 [Lee, C., Martin, R. V., van Donkelaar, A., Lee, H., Dickerson, R. R., Hains, J. C., Krotkov, N., Richter, A., Vinnikov, K., and](#)
1171 [Schwab, J. J.: SO₂ emissions and lifetimes: Estimates from inverse modeling using in situ and global, space-based](#)
1172 [\(SCIAMACHY and OMI\) observations, *J. Geophys. Res.-Atmos.*, 116, D06304, <https://doi.org/10.1029/2010JD014758>,](#)
1173 [2011.](#)
- 1174 McKee, M. L.: Theoretical study of the CH₃SOO radical, *Chemical Physics Letters*, 211, 643–648,
1175 [https://doi.org/10.1016/0009-2614\(93\)80157-K](https://doi.org/10.1016/0009-2614(93)80157-K), 1993.
- 1176 Minikin, A., Legrand, M., Hall, J., Wagenbach, D., Kleefeld, C., Wolff, E., Pasteur, E. C., and Ducroz, F.: Sulfur-containing
1177 species (sulfate and methanesulfonate) in coastal Antarctic aerosol and precipitation, 103, 10975–10990,
1178 <https://doi.org/10.1029/98JD00249>, 1998.
- 1179 Mulcahy, J.P., Jones, C., Sellar, A., Johnson, B., Boutle, I.A., Jones, A., Andrews, T., Rumbold, S.T., Mollard, J., Bellouin,
1180 N. and Johnson, C.E. Improved aerosol processes and effective radiative forcing in HadGEM3 and UKESM1. *Journal of*
1181 *Advances in Modeling Earth Systems*, 10(11), pp.2786-2805. 2018.
- 1182 Mulcahy, J. P., Johnson, C., Jones, C. G., Povey, A. C., Scott, C. E., Sellar, A., Turnock, S. T., Woodhouse, M. T., Abraham,
1183 N. L., Andrews, M. B., Bellouin, N., Browse, J., Carslaw, K. S., Dalvi, M., Folberth, G. A., Glover, M., Grosvenor, D. P.,
1184 Hardacre, C., Hill, R., Johnson, B., Jones, A., Kipling, Z., Mann, G., Mollard, J., O'Connor, F. M., Palmiéri, J., Reddington,
1185 C., Rumbold, S. T., Richardson, M., Schutgens, N. A. J., Stier, P., Stringer, M., Tang, Y., Walton, J., Woodward, S., and Yool,
1186 A.: Description and evaluation of aerosol in UKESM1 and HadGEM3-GC3.1 CMIP6 historical simulations, 13, 6383–6423,
1187 <https://doi.org/10.5194/gmd-13-6383-2020>, 2020.
- 1188 Novak, G. A., Fite, C. H., Holmes, C. D., Veres, P. R., Neuman, J. A., Faloona, I., Thornton, J. A., Wolfe, G. M., Vermeuel,
1189 M. P., Jernigan, C. M., Peischl, J., Ryerson, T. B., Thompson, C. R., Bourgeois, I., Warneke, C., Gkatzelis, G. I., Coggon, M.
1190 M., Sekimoto, K., Bui, T. P., Dean-Day, J., Diskin, G. S., DiGangi, J. P., Nowak, J. B., Moore, R. H., Wiggins, E. B., Winstead,
1191 E. L., Robinson, C., Thornhill, K. L., Sanchez, K. J., Hall, S. R., Ullmann, K., Dollner, M., Weinzierl, B., Blake, D. R., and
1192 Bertram, T. H.: Rapid cloud removal of dimethyl sulfide oxidation products limits SO₂ and cloud condensation nuclei
1193 production in the marine atmosphere, *PNAS*, 118, <https://doi.org/10.1073/pnas.2110472118>, 2021.

Development and intercomparison of DMS oxidation mechanisms

- 1194 Pacifico, F., Harrison, S. P., Jones, C. D., Arneth, A., Sitch, S., Weedon, G. P., Barkley, M. P., Palmer, P. I., Serça, D.,
1195 Potosnak, M., Fu, T.-M., Goldstein, A., Bai, J., and Schurgers, G.: Evaluation of a photosynthesis-based biogenic isoprene
1196 emission scheme in JULES and simulation of isoprene emissions under present-day climate conditions, 11, 4371–4389,
1197 <https://doi.org/10.5194/acp-11-4371-2011>, 2011.
- 1198 Pham, M., Müller, J.-F., Brasseur, G. P., Granier, C., and Mégie, G.: A three-dimensional study of the tropospheric sulfur
1199 cycle, 100, 26061–26092, <https://doi.org/10.1029/95JD02095>, 1995.
- 1200 Ranjithkumar, A., Gordon, H., Williamson, C., Rollins, A., Pringle, K., Kupc, A., Abraham, N. L., Brock, C., and Carslaw,
1201 K.: Constraints on global aerosol number concentration, SO₂ and condensation sink in UKESM1 using ATom measurements,
1202 *Atmos. Chem. Phys.*, 21, 4979–5014, <https://doi.org/10.5194/acp-21-4979-2021>, 2021.
- 1203 [Sander, R.: Compilation of Henry's law constants \(version 4.0\) for water as solvent, *Atmos. Chem. Phys.*, 15, 4399–4981,](https://doi.org/10.5194/acp-15-4399-2015)
1204 <https://doi.org/10.5194/acp-15-4399-2015>, 2015, [corrigendum, 2021](https://doi.org/10.5194/acp-15-4399-2015).
- 1205 Sandu, A. and Sander, R.: Technical note: Simulating chemical systems in Fortran90 and Matlab with the Kinetic PreProcessor
1206 KPP-2.1, 6, 187–195, <https://doi.org/10.5194/acp-6-187-2006>, 2006.
- 1207 Sciare, J., Mihalopoulos, N., and Dentener, F. J.: Interannual variability of atmospheric dimethylsulfide in the southern Indian
1208 Ocean, *J. Geophys. Res.*, 105, 26369–26377, <https://doi.org/10.1029/2000JD900236>, 2000.
- 1209 Sciare, J., Baboukas, E., and Mihalopoulos, N.: Short-Term Variability of Atmospheric DMS and Its Oxidation Products at
1210 Amsterdam Island during Summer Time, *Journal of Atmospheric Chemistry*, 39, 281–302,
1211 <https://doi.org/10.1023/A:1010631305307>, 2001.
- 1212 Sellar, A. A., Jones, C. G., Mulcahy, J. P., Tang, Y., Yool, A., Wiltshire, A., O'Connor, F. M., Stringer, M., Hill, R., Palmieri,
1213 J., Woodward, S., Mora, L. de, Kuhlbrodt, T., Rumbold, S. T., Kelley, D. I., Ellis, R., Johnson, C. E., Walton, J., Abraham, N.
1214 L., Andrews, M. B., Andrews, T., Archibald, A. T., Berthou, S., Burke, E., Blockley, E., Carslaw, K., Dalvi, M., Edwards, J.,
1215 Folberth, G. A., Gedney, N., Griffiths, P. T., Harper, A. B., Hendry, M. A., Hewitt, A. J., Johnson, B., Jones, A., Jones, C. D.,
1216 Keeble, J., Liddicoat, S., Morgenstern, O., Parker, R. J., Predoi, V., Robertson, E., Sahaan, A., Smith, R. S., Swaminathan,
1217 R., Woodhouse, M. T., Zeng, G., and Zerroukat, M.: UKESM1: Description and Evaluation of the U.K. Earth System Model,
1218 11, 4513–4558, <https://doi.org/10.1029/2019MS001739>, 2019.
- 1219 Sellar, A. A., Walton, J., Jones, C. G., Wood, R., Abraham, N. L., Andrejczuk, M., Andrews, M. B., Andrews, T., Archibald,
1220 A. T., de Mora, L., Dyson, H., Elkington, M., Ellis, R., Florek, P., Good, P., Gohar, L., Haddad, S., Hardiman, S. C., Hogan,
1221 E., Iwi, A., Jones, C. D., Johnson, B., Kelley, D. I., Kettleborough, J., Knight, J. R., Köhler, M. O., Kuhlbrodt, T., Liddicoat,
1222 S., Linova-Pavlova, I., Mizielinski, M. S., Morgenstern, O., Mulcahy, J., Neiningner, E., O'Connor, F. M., Petrie, R., Ridley,
1223 J., Rioual, J.-C., Roberts, M., Robertson, E., Rumbold, S., Seddon, J., Shepherd, H., Shim, S., Stephens, A., Teixeira, J. C.,
1224 Tang, Y., Williams, J., Wiltshire, A., and Griffiths, P. T.: Implementation of U.K. Earth System Models for CMIP6, 12,
1225 e2019MS001946, <https://doi.org/10.1029/2019MS001946>, 2020.

Development and intercomparison of DMS oxidation mechanisms

- 1226 Stevenson, D. S., Zhao, A., Naik, V., O'Connor, F. M., Tilmes, S., Zeng, G., Murray, L. T., Collins, W. J., Griffiths, P. T.,
1227 Shim, S., Horowitz, L. W., Sentman, L. T., and Emmons, L.: Trends in global tropospheric hydroxyl radical and methane
1228 lifetime since 1850 from AerChemMIP, *Atmos. Chem. Phys.*, 20, 12905–12920, <https://doi.org/10.5194/acp-20-12905-2020>,
1229 2020.
- 1230 Sutton, R.T., McCarthy, G.D., Robson, J., Sinha, B., Archibald, A.T. and Gray, L.J. Atlantic multidecadal variability and the
1231 UK ACSIS program. *Bulletin of the American Meteorological Society*, 99(2), pp.415-425. 2018.
- 1232 Telford, P. J., Abraham, N. L., Archibald, A. T., Braesicke, P., Dalvi, M., Morgenstern, O., O'Connor, F. M., Richards, N. a.
1233 D., and Pyle, J. A.: Implementation of the Fast-JX Photolysis scheme (v6.4) into the UKCA component of the MetUM
1234 chemistry-climate model (v7.3), 6, 161–177, <https://doi.org/10.5194/gmd-6-161-2013>, 2013.
- 1235 Tesdal, J.-E., Christian, J. R., Monahan, A. H., Salzen, K. von, Tesdal, J.-E., Christian, J. R., Monahan, A. H., and Salzen, K.
1236 von: Evaluation of diverse approaches for estimating sea-surface DMS concentration and air–sea exchange at global scale,
1237 *Environ. Chem.*, 13, 390–412, <https://doi.org/10.1071/EN14255>, 2015.
- 1238 Thomas, E.R., Allen, C.S., Etourneau, J., King, A.C., Severi, M., Winton, V.H.L., Mueller, J., Crosta, X. and Peck, V.L.
1239 Antarctic sea ice proxies from marine and ice core archives suitable for reconstructing sea ice over the past 2000 years.
1240 *Geosciences*, 9(12), 506. 2019.
- 1241 Turnipseed, A. A., Barone, S. B., and Ravishankara, A. R.: Observation of methylthiyl radical addition to oxygen in the gas
1242 phase, *J. Phys. Chem.*, 96, 7502–7505, <https://doi.org/10.1021/j100198a006>, 1992.
- 1243 Urbanski, S. P., Stickel, R. E., and Wine, P. H.: Mechanistic and Kinetic Study of the Gas-Phase Reaction of Hydroxyl Radical
1244 with Dimethyl Sulfoxide, *J. Phys. Chem. A*, 102, 10522–10529, <https://doi.org/10.1021/jp9833911>, 1998.
- 1245 Veres, P. R., Neuman, J. A., Bertram, T. H., Assaf, E., Wolfe, G. M., Williamson, C. J., Weinzierl, B., Tilmes, S., Thompson,
1246 C. R., Thames, A. B., Schroder, J. C., Saiz-Lopez, A., Rollins, A. W., Roberts, J. M., Price, D., Peischl, J., Nault, B. A., Møller,
1247 K. H., Miller, D. O., Meinardi, S., Li, Q., Lamarque, J.-F., Kupc, A., Kjaergaard, H. G., Kinnison, D., Jimenez, J. L., Jernigan,
1248 C. M., Hornbrook, R. S., Hills, A., Dollner, M., Day, D. A., Cuevas, C. A., Campuzano-Jost, P., Burkholder, J., Bui, T. P.,
1249 Brune, W. H., Brown, S. S., Brock, C. A., Bourgeois, I., Blake, D. R., Apel, E. C., and Ryerson, T. B.: Global airborne sampling
1250 reveals a previously unobserved dimethyl sulfide oxidation mechanism in the marine atmosphere, *Proc Natl Acad Sci USA*,
1251 117, 4505–4510, <https://doi.org/10.1073/pnas.1919344117>, 2020.
- 1252 Vermeuel, M. P., Novak, G. A., Jernigan, C. M., and Bertram, T. H.: Diel Profile of Hydroperoxymethyl Thioformate:
1253 Evidence for Surface Deposition and Multiphase Chemistry, *Environ. Sci. Technol.*, 54, 12521–12529,
1254 <https://doi.org/10.1021/acs.est.0c04323>, 2020.
- 1255 [von Glasow, R. and Crutzen, P. J.: Model study of multiphase DMS oxidation with a focus on halogens, *Atmos. Chem. Phys.*,
1256 4, 589–608, <https://doi.org/10.5194/acp-4-589-2004>, 2004.](#)

Development and intercomparison of DMS oxidation mechanisms

- 1257 Walters, D., Baran, A. J., Boutle, I., Brooks, M., Earnshaw, P., Edwards, J., Furtado, K., Hill, P., Lock, A., Manners, J.,
1258 Morcrette, C., Mulcahy, J., Sanchez, C., Smith, C., Stratton, R., Tennant, W., Tomassini, L., Van Weverberg, K., Vosper, S.,
1259 Willett, M., Browse, J., Bushell, A., Carslaw, K., Dalvi, M., Essery, R., Gedney, N., Hardiman, S., Johnson, B., Johnson, C.,
1260 Jones, A., Jones, C., Mann, G., Milton, S., Rumbold, H., Sellar, A., Ujiie, M., Whitall, M., Williams, K., and Zerroukat, M.:
1261 The Met Office Unified Model Global Atmosphere 7.0/7.1 and JULES Global Land 7.0 configurations, 12, 1909–1963,
1262 <https://doi.org/10.5194/gmd-12-1909-2019>, 2019.
- 1263 Wang, X., Jacob, D. J., Downs, W., Zhai, S., Zhu, L., Shah, V., Holmes, C. D., Sherwen, T., Alexander, B., Evans, M. J.,
1264 Eastham, S. D., Neuman, J. A., Veres, P. R., Koenig, T. K., Volkamer, R., Huey, L. G., Bannan, T. J., Percival, C. J., Lee, B.
1265 H., and Thornton, J. A.: Global tropospheric halogen (Cl, Br, I) chemistry and its impact on oxidants, 21, 13973–13996,
1266 <https://doi.org/10.5194/acp-21-13973-2021>, 2021.
- 1267 Weber, J., Archer-Nicholls, S., Griffiths, P., Berndt, T., Jenkin, M., Gordon, H., Knote, C., and Archibald, A. T.: CRI-HOM:
1268 A novel chemical mechanism for simulating highly oxygenated organic molecules (HOMs) in global chemistry–aerosol–
1269 climate models, *Atmos. Chem. Phys.*, 20, 10889–10910, <https://doi.org/10.5194/acp-20-10889-2020>, 2020.
- 1270 Weber, J., Archer-Nicholls, S., Abraham, N. L., Shin, Y. M., Bannan, T. J., Percival, C. J., Bacak, A., Artaxo, P., Jenkin, M.,
1271 Khan, M. A. H., Shallcross, D. E., Schwantes, R. H., Williams, J., and Archibald, A. T.: Improvements to the representation
1272 of BVOC chemistry–climate interactions in UKCA (v11.5) with the CRI-Strat 2 mechanism: incorporation and evaluation, 14,
1273 5239–5268, <https://doi.org/10.5194/gmd-14-5239-2021>, 2021.
- 1274 Wells, K.C., Millet, D.B., Payne, V.H., Deventer, M.J., Bates, K.H., de Gouw, J.A., Graus, M., Warneke, C., Wisthaler, A.
1275 and Fuentes, J.D. Satellite isoprene retrievals constrain emissions and atmospheric oxidation. *Nature*, 585(7824), 225–233.
1276 2020.
- 1277 [Wennberg, P. O., Bates, K. H., Crounse, J. D., Dodson, L. G., McVay, R. C., Mertens, L. A., Nguyen, T. B., Praske, E.,](#)
1278 [Schwantes, R. H., Smarte, M. D., St Clair, J. M., Teng, A. P., Zhang, X., and Seinfeld, J. H.: Gas-Phase reactions of isoprene](#)
1279 [and its major oxidation products, *Chem. Rev.*, 118, 3337–3390, <https://doi.org/10.1021/acs.chemrev.7b00439>, 2018.](#)
- 1280 Wofsy, S. C., Afshar, S., Allen, H. M., Apel, E. C., Asher, E. C., Barletta, B., Bent, J., Bian, H., Biggs, B. C., Blake, D. R.,
1281 Blake, N., Bourgeois, I., Brock, C. A., Brune, W. H., Budney, J. W., Bui, T. P., Butler, A., Campuzano-Jost, P., Chang, C. S.,
1282 Chin, M., Commane, R., Corr, G., and Zeng, L. H.: ATom: merged atmospheric chemistry, trace gases, and aerosols, data set,
1283 ORNL DAAC, Oak Ridge, Tennessee, USA, <https://doi.org/10.3334/ORNLDAAC/1581>, 2018.
- 1284 Wollesen de Jonge, R., Elm, J., Rosati, B., Christiansen, S., Hyttinen, N., Lüdemann, D., Bilde, M., and Roldin, P.: Secondary
1285 aerosol formation from dimethyl sulfide – improved mechanistic understanding based on smog chamber experiments and
1286 modelling, 21, 9955–9976, <https://doi.org/10.5194/acp-21-9955-2021>, 2021.

Development and intercomparison of DMS oxidation mechanisms

1287 Wu, R., Wang, S., and Wang, L.: New Mechanism for the Atmospheric Oxidation of Dimethyl Sulfide. The Importance of
1288 Intramolecular Hydrogen Shift in a $\text{CH}_3\text{SCH}_2\text{OO}$ Radical, *J. Phys. Chem. A*, 119, 112–117, <https://doi.org/10.1021/jp511616j>,
1289 2015.

1290 Ye, Q., Goss, M. B., Isaacman-VanWertz, G., Zaytsev, A., Massoli, P., Lim, C., Croteau, P., Canagaratna, M., Knopf, D. A.,
1291 Keutsch, F. N., Heald, C. L., and Kroll, J. H.: Organic Sulfur Products and Peroxy Radical Isomerization in the OH Oxidation
1292 of Dimethyl Sulfide, *ACS Earth Space Chem.*, <https://doi.org/10.1021/acsearthspacechem.1c00108>, 2021.
1293